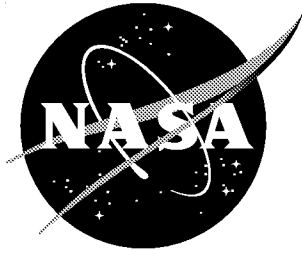NASA/TM-1999-209357

Aerodynamic Characteristics and Control Effectiveness of the HL-20 Lifting Body Configuration at Mach 10 in Air

William I. Scallion
Langley Research Center, Hampton, Virginia

September 1999

The NASA STI Program Office ... in Profile

Since its founding, NASA has been dedicated to the advancement of aeronautics and space science. The NASA Scientific and Technical Information (STI) Program Office plays a key part in helping NASA maintain this important role.

The NASA STI Program Office is operated by Langley Research Center, the lead center for NASA's scientific and technical information. The NASA STI Program Office provides access to the NASA STI Database, the largest collection of aeronautical and space science STI in the world. The Program Office is also NASA's institutional mechanism for disseminating the results of its research and development activities. These results are published by NASA in the NASA STI Report Series, which includes the following report types:
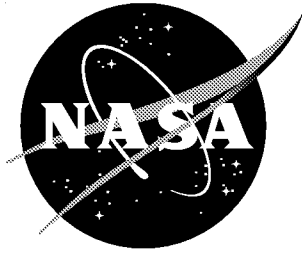
- TECHNICAL PUBLICATION. Reports of completed research or a major significant phase of research that present the results of NASA programs and include extensive data or theoretical analysis. Includes compilations of significant scientific and technical data and information deemed to be of continuing reference value. NASA counterpart of peer-reviewed formal professional papers, but having less stringent limitations on manuscript length and extent of graphic presentations.

- TECHNICAL MEMORANDUM. Scientific and technical findings that are preliminary or of specialized interest, e.g., quick release reports, working papers, and bibliographies that contain minimal annotation. Does not contain extensive analysis.

- CONTRACTOR REPORT. Scientific and technical findings by NASA-sponsored contractors and grantees.

- CONFERENCE PUBLICATION. Collected papers from scientific and technical conferences, symposia, seminars, or other meetings sponsored or co-sponsored by NASA.

- SPECIAL PUBLICATION. Scientific, technical, or historical information from NASA programs, projects, and missions, often concerned with subjects having substantial public interest.

- TECHNICAL TRANSLATION. English-language translations of foreign scientific and technical material pertinent to NASA's mission.

Specialized services that complement the STI Program Office's diverse offerings include creating custom thesauri, building customized databases, organizing and publishing research results ... even providing videos.

For more information about the NASA STI Program Office, see the following:

- Access the NASA STI Program Home Page at *http://www.sti.nasa.gov*

- E-mail your question via the Internet to help@sti.nasa.gov

- Fax your question to the NASA STI Help Desk at (301) 621-0134

- Phone the NASA STI Help Desk at (301) 621-0390

- Write to:
  NASA STI Help Desk
  NASA Center for AeroSpace Information
  7121 Standard Drive
  Hanover, MD 21076-1320

Aerodynamic Characteristics and Control Effectiveness of the HL-20 Lifting Body Configuration at Mach 10 in Air

William I. Scallion
Langley Research Center, Hampton, Virginia

September 1999

Aerodynamic Characteristics and Control Effectiveness of
the HL-20 Lifting Body Configuration at Mach 10 in Air

By
William I. Scallion
Langley Research Center

ABSTRACT

A 0.0196-scale model of the HL-20 lifting-body, one of several configurations proposed for future crewed spacecraft, was tested in the Langley 31-Inch Mach 10 Tunnel. The purpose of the tests was to determine the effectiveness of fin-mounted elevons, a lower surface flush-mounted body flap, and a flush-mounted yaw controller at hypersonic speeds. The nominal angle-of-attack range, representative of hypersonic entry, was 20° to 41°, the sideslip angles were 0°, 2°, and -2°, and the test Reynolds number was 1.06 x 10^6 based on model reference length. The aerodynamic, longitudinal, and lateral control effectiveness along with surface oil flow visualizations are presented and discussed. The configuration was longitudinally and laterally stable at the nominal center of gravity. The primary longitudinal control, the fin-mounted elevons, could not trim the model to the desired entry angle of attack of 30°. The lower surface body flaps were effective for roll control and the associated adverse yawing moment was eliminated by skewing the body flap hinge lines. A yaw controller, flush-mounted on the lower surface, was also effective, and the associated small rolling moment was favorable.

SUMMARY

A 0.0196-scale model of the HL-20 lifting body spacecraft configuration was tested in the Langley 31-Inch Mach 10 Tunnel to determine the aerodynamic stability and control characteristics at hypersonic speeds. Measurements of aerodynamic forces and moments were obtained for the configuration with fin-mounted elevons, lower surface body flaps with a conventional and a skewed hinge line, and a triangular-shaped yaw controller flush-mounted on the lower surface. The configuration was tested over a nominal angle-of-attack range of 20° to 41° at sideslip angles of 0°, 2°, and -2° at a nominal Mach number of 10 and a Reynolds number of 1.06 x 10^6 based on model reference length.

The results indicated that for the given center-of-gravity location of 54 percent of the reference body length, the configuration was statically stable longitudinally and laterally. The fin-mounted elevons, the primary longitudinal controls, were ineffective and could not trim the configuration above an angle of attack of 23.5°. The conventional body flap was an effective roll control, and the associated adverse yawing moment was eliminated by skewing the hinge line 25°. The yaw controller was also effective and the associated rolling moment was slightly favorable. Both the lower-surface body flap and yaw controller, when deflected for roll and yaw respectively, produced adverse pitching moments larger than the trim capability of the fin-mounted elevons.

INTRODUCTION

A permanently crewed space station orbiting the Earth places additional requirements on the existing capability to transport personnel to and from orbit. A prime consideration is the return of personnel to Earth in the event of an emergency. An additional consideration is the routine, economical transportation of personnel to and from the station to supplement the space shuttle capability. The National Aeronautics and Space Administration has been investigating a number of possible crewed spacecraft configurations designed to meet these requirements. One of the configurations is a lifting body designated the HL-20 (ref. 1). This configuration has been tested in wind tunnels to determine its aerodynamic characteristics throughout the speed range from subsonic to hypersonic conditions (refs. 2 to 9). The control characteristics were investigated at subsonic speeds (ref. 9), transonic speeds (ref. 6), and supersonic speeds (refs. 7 and 8).

The present tests were performed to obtain the effectiveness of the HL-20 controls at hypersonic speeds. The tests were conducted in the Langley 31-Inch Mach 10 Tunnel with a 0.0196 scale model at a nominal Mach number of 10, and a free stream unit Reynolds number per foot of 2.2×10^6 corresponding to a length Reynolds number of 1.06×10^6. Control effectiveness data were obtained for the fin-mounted elevons, the lower-surface body flap with a conventional and a skewed hinge line, and a lower-surface triangular-shaped yaw controller. The model was tested over a nominal angle-of-attack range of 20° to 41° at zero sideslip and sideslip angles of 2° and -2°.

SYMBOLS

The aerodynamic data are referenced to the body axis system (fig. 1). The coefficients are based on the planform area, length, and span of the body without fins. The moment center is located at a station 54 percent of the body length from the nose and 8 percent of the body length above the flat lower surface.

b	reference body span, 2.826 in.
C_A	axial force coefficient, Axial force/$(q_\infty \times S_{ref})$
C_D	drag coefficient, Drag/$(q_\infty \times S_{ref})$
C_L	lift coefficient, Lift/$(q_\infty \times S_{ref})$
C_l	rolling-moment coefficient, Rolling-moment/$(q_\infty \times S_{ref} \times b)$
$C_{l\beta}$	$= \partial C_l / \partial \beta$, taken at $\beta = -2°$ and 2°, per degree
C_m	pitching-moment coefficient, Pitching moment/$(q_\infty \times S_{ref} \times l)$
C_n	yawing-moment coefficient, Yawing moment/$(q_\infty \times S_{ref} \times b)$
$C_{n\beta}$	$= \partial C_n / \partial \beta$, taken at $\beta = -2°$ and 2°, per degree
C_p	pressure coefficient, $(p_{local} - p_{inf})/q_\infty$
C_Y	side-force coefficient, Side force/$(q_\infty \times S_{ref})$
$C_{Y\beta}$	$= \partial C_Y / \partial \beta$, taken at $\beta = 2°$ and -2°, per degree
L/D	lift-drag ratio
l	reference body length, 5.772 in.
p	pressure, psi
q_∞	free-stream dynamic pressure, psi

R	Reynolds number
S_{ref}	basic body planform area (excluding fins), 11.9088 in^2
X	longitudinal body axis, positive forward
Y	lateral body axis, positive to the right
Z	vertical body axis, positive downward
x, y, z	coordinates of X, Y and Z axes, respectively
α	angle of attack, deg.
β	angle of sideslip, deg.
Δ	increment
δ_{BF}	body-flap deflection angle, positive downward, deg.
U	coefficient uncertainty based on balance resolution
δ_e	tip fin elevon deflection angle, positive downward, deg.
δ_y	yaw controller deflection angle, deg.

Subscripts:

L	left
∞	free stream

APPARATUS AND TESTS

Model

The model used in the tests reported herein was a 0.0196-scale cast stainless steel model used in the tests of reference 4. This model was modified for the present test by providing the aerodynamic controls for hypersonic entry flight consisting of the fin-mounted elevons and the lower surface flush-mounted body flaps. Additionally, an aerodynamic yaw control device was designed for the present test that is described in a subsequent section. Sketches of the model are presented in figure 2, and photographs of the model and a full-scale mockup are presented in figure 3. The configuration consisted of a low-fineness-ratio body with a flat undersurface, a blunted nose, a small center fin, and two outboard fins set at a dihedral angle of 50°. The model was a thin-walled stainless steel casting without final machining to gain high fidelity; however, since the purpose of the tests reported herein was to obtain the incremental effects of the aerodynamic controls, some model asymmetries could be tolerated. Subsequent to the tests, the model surfaces were measured in order to assess effects of any asymmetries on the basic aerodynamic characteristics. These measurements revealed that the nose and aft end of the model were displaced in the positive Y-direction, with the aft end displaced the most. Along the length of the body, the displacement tended to be to the left, or the negative Y-direction. These displacements, ranging from Y = -0.018 to 0.016 inches, illustrated that the model was warped, or cambered in the Y-plane, and oriented slightly nose left. This effective camber and nose left orientation, however small, would tend to produce a negative increment in side-force coefficient, and a positive increment in yawing-moment coefficient. It would also tend to produce a negative increment in rolling-moment coefficient, but the measurements also showed that the right fin had 1.28° more negative incidence than the left fin, which would produce a roll to the right, or a positive rolling-moment increment. As will be shown subsequently, the basic lateral data tended to reflect these differences from the specified

outer mold lines but it is believed that they did not substantially influence the incremental control effectiveness.

Controls

The control of the HL-20 during atmospheric entry is accomplished by a combination of movable aerodynamic surfaces and a three-axis reaction control system (RCS). Reference 10 states that the pitch and roll RCS are active until the dynamic pressure reaches 50 psf, and the yaw RCS remains active for yaw control until the Mach number decreases to 3.5. All aerodynamic surfaces, except the rudder, become active at a dynamic pressure 2 psf, and the rudder is activated at a Mach number of 3.5.

The control system was designed to use the fin-mounted elevons for pitch control augmented by the upper body flaps, the lower body flaps for roll control, the RCS and rudder for yaw control, and the upper and lower body flaps deflected simultaneously as a speed brake (ref. 10). The control geometry of references 8 and 9 were used to design the control configuration for the present tests.

The model fins were modified to include trailing-edge elevons (figs. 2(b) and 2(c)) scaled from those described in reference 8. The elevons were provided with brackets for deflections of 0°, 10°, 20°, 40° -10°, -20° and -40°. The model was also provided with lower surface body flaps (ref. 8) having deflection angles of 10° and 20° (fig. 2(d)). Because the drag of the deflected body flap on the lower surface would be expected to produce adverse yawing moments, two additional body flaps with the hinge lines skewed 25° from the Y-axis direction were fabricated to compensate for this with deflections of 15° and 30° (fig. 2(d)). As the HL-20 had no direct hypersonic aerodynamic yaw control, a bottom-surface yaw control shown to be effective in reference 11 for the Shuttle orbiter was fabricated for the present test (figs. 2(e) and 3(d)). This control concept is unconventional in that the hinge line is swept 60°, and the control lies flush with the vehicle bottom surface when undeflected. The control would be deflected 0° to 90° to provide yaw control during entry. When undeflected, the control leading edges lie parallel to the vehicle centerline, and their trailing edges coincide with the vehicle trailing edge. At 90° deflection, the control leading edge is swept 60°. Controls fabricated for the present study include deflections of 45° and 90°. Upper surface body flaps were not provided for this test because reference 8 indicated that at high angles of attack at Mach 4.5, the upper surface controls were not effective.

Facility and Instrumentation

The Langley 31-Inch Mach 10 Tunnel expands heated dry air through a three-dimensional, square, contoured nozzle into a 31-inch square test section. The nominal test Mach number is 10. The tunnel operates in the blowdown mode with run times ranging from 60 to 120 seconds. The air is heated to approximately 1850° R by an electrical resistance heater with reservoir pressures up to approximately 1500 psia. Average free stream flow conditions for this test were a static pressure of 0.0349 psi and a dynamic pressure of 2.43 psi at a temperature of 90.7° R. The free stream velocity was 4642 ft./sec. resulting in a Mach number of 9.937 and a Reynolds number of 2.22×10^6 per ft. (1.06×10^6 based on model reference length). The value of the viscous interaction

parameter was 0.0084. Models are supported on a hydraulically-operated, sidewall-mounted injection system. This tunnel and its capabilities are described in more detail in reference 12.

The force and moment data were recorded with a six-component water-cooled, internally mounted strain gage balance. Balance internal temperatures were monitored with two thermocouples installed in the surrounding water jacket. The model and balance were supported on a sting at the base of the model (fig. 3(a)). The model angles of attack and sideslip were varied by rotating the tunnel sting support system in the pitch plane and in the yaw plane relative to the pitch plane. The yaw plane of the model rotates with the model; therefore, sideslip angle β varies slightly with angle of attack. Angle of attack and yaw are measured by transducers in the tunnel support system. The sideslip angle was corrected for the variation of yaw angle with angle of attack; angle of attack and sideslip were corrected for sting and balance deflections under load. The force and moment data were corrected for weight tares. Base pressures were measured but no corrections for them were applied to the axial force data.

Model Test Methods

The force and moment tests were conducted for an angle-of-attack range of 20° to 41° at zero, 2°, and -2° sideslip angles at a unit Reynolds number of 2.2 million per foot (1.06 million based on model reference length). The model angle of attack was varied using the pitch-pause technique. During the tests only the left-hand controls were deflected. The body flaps and the bottom-surface-mounted yaw controller were tested to obtain lateral control effectiveness data; the elevons were tested both for longitudinal and lateral control, and the longitudinal control effectiveness was obtained by adding the incremental effects of the single control to the data obtained with one control. This procedure for the elevons was validated in reference 8. Oil-flow visualizations of the lower model surface were recorded on photographic film at alpha = 20° and 30° for several control deflections.

Uncertainties

The calibration accuracy of the strain gage balance is 0.25 percent of the design load rating of the six components and the related uncertainties in the corresponding coefficients are listed below:

C_N	C_A	C_Y	C_m	C_n	C_l
±0.00352	±0.000264	±0.00044	±0.00090	±0.00029	±0.000156

The moment coefficient uncertainties caused by balance calibration accuracies include those in the force coefficients used in the moment transfer equations. For example, U_{Cm} (total) = U_{Cm} (measured) + U_{CN} ($\Delta x/l$), where Δx is the transfer distance. Because of the relatively large moment transfer distance ($X/l = .126$) associated with the existing model, these inclusions essentially doubled the uncertainties in C_m and C_n. This adversely affected the longitudinal control effectiveness data in the present case, because the effectiveness in pitch control was obtained by doubling the incremental

effectiveness of a single elevon. This in turn doubled the effect of balance normal force accuracy on the resulting increment. Because the increments obtained in the present investigation were small, the uncertainties caused by balance accuracies could be as large as the increments produced by deflecting the control.

RESULTS AND DISCUSSION

Presentation of Data

The static longitudinal and lateral aerodynamic characteristics of the basic HL-20 model with all controls at zero deflection are presented in figures 4 to 6. The model is longitudinally stable in the angle-of-attack range tested (fig. 4(b)). The effects of sideslip on the lateral-directional characteristics of the model are shown in figure 5. The offsets in the lateral parameters at zero sideslip reflect the trends discussed previously in the section on model asymmetries. The model is laterally and directionally stable through the angle-of-attack range tested (figs. 5 and 6). The effects of elevon deflection on longitudinal characteristics are shown in figure 7. The lateral control effects at several control deflections as functions of angle of attack are given in figures 8 to 11 for the conventional left body flap, the left body flap with the hinge line skewed 25° (see fig. 2(d)), and the left-hand yaw controller. The lateral control effectiveness of the body flaps and yaw controller are shown in figures 12 to 14 and figure 16 as a function of control deflection for several angles of attack. Surface oil-flow photographs with the body flaps and yaw controller deflected are presented in figures 15 and 17 respectively.

Longitudinal Control Characteristics

Figure 4(b) shows that with the elevons undeflected, the model is longitudinally trimmed at an angle of attack of 22.5°. Combining the incremental data for a single elevon at $\delta_e = -40°$ to represent the effect of both elevons at -40° increases the trim angle of attack to about 23.5° (fig. 7(b)). Although considerable scatter is evident in the data, the end result is not significantly affected; the control effectiveness of the upward-deflected elevons as indicated by the limited trim angle of attack range is minimal. According to reference 10, the nominal entry angle of attack for the HL-20 is 30° from entry interface at an altitude of 400,000 feet to an altitude of 157,000 feet and a Mach number of 10. Based on the data reported herein, the vehicle has insufficient hypersonic longitudinal trim capability to fly the desired entry trajectory with the present c.g. location. The vehicle is quite stable longitudinally because of the forward-located center of gravity. The vehicle longitudinal stability can be reduced in two ways: one, shift the center of gravity aft, and two, shift the aerodynamic center of pressure forward. The center of gravity can be shifted aft by moving internal components, but this is limited to those that can be practically moved such as batteries and propellant tanks, and by providing ballast, but the added weight may be limited by performance considerations. The center of pressure can be moved forward by reshaping the body and fin planforms and/or moving the fins forward. Additionally, the longitudinal trim capability can be improved by reshaping the body profile to provide negative camber (positive increment in C_m with little change in longitudinal stability) and/or increasing the size of the elevons; however, either revision will result in a loss in trim lift. The loss

in some trim lift can be tolerated at hypersonic speeds, since a high trim angle of attack in this regime is more important because of aeroheating. However, the decreased trim lift can become critical at transonic and subsonic speeds. The effect of body camber on the lift and moment characteristics of the HL-20 at subsonic speeds is shown in reference 13. It is believed that with a judicious combination of the approaches discussed above, the vehicle can be modified to trim to the desired angle of attack at hypersonic speeds. However, the impact of the modifications on the aerodynamic characteristics must be considered for the entire entry speed range. Upper surface body flaps are not a valid consideration at high angles of attack, because the lee-side flow field has insufficient momentum to make these controls effective. Reference 8 shows that the upper surface body flaps are essentially ineffective above Mach 3 at high angles of attack.

<div align="center">Lateral Control Characteristics</div>

The primary roll control of the HL-20 would be provided by the lower surface body flaps (see fig. 2(d)). The conventional body flap (hinge line parallel to the Y axis) has adequate rolling effectiveness as shown in figure 12. A calculation of the roll angular acceleration at Mach 20 flight conditions for the nominal trajectory and the inertial data from reference 10 gives a value of 12.5 deg/sec^2 for a body flap deflection of 20°. This is accompanied by pitching moments larger than the trim capability of the elevons, and by adverse yawing moments (calculated value of 769 ft.-lb. at Mach 20). The adverse yawing moments can be eliminated by a judicious choice of skew angle for the body flap hinge. Figure 13 shows the roll control effectiveness of a body flap with the hinge line skewed 25° relative to the Y-axis (see the right side of fig. 2(d)). The skew angle of 25° was calculated to eliminate the adverse yaw caused by deflection of the control for roll. The data of figure 13 show that the resulting yawing-moment coefficient is slightly positive; i.e., a favorable yawing moment. The 15° and 30° deflection angles were chosen with the expectation that the skewed control would not be as effective in roll as the conventional body flap. A comparison of the effectiveness of the two body flap configurations at an angle of attack of 40° (fig. 14) shows that the body flap is less effective in roll, but by a lesser amount than was anticipated. Note the large difference in yawing-moment coefficient produced by the controls; the negative (adverse) yawing moment produced by the conventional body flap becomes positive (favorable) when the hinge line is skewed. A slight adjustment in the skew angle would eliminate the yawing moment altogether. As expected, the side force produced by the skewed body flap is larger than that produced by the conventional body flap. Both controls, when deflected, produced about the same pitching-moments; either control increases the longitudinal out-of-trim moment.

Photographs of surface oil-flow patterns with the body flaps deflected (fig. 15) illustrate the high pressure region generated on the lower surface in the area ahead of the control hinge line. This can be seen in figure 15(a) where the flow is directed around the ends of the control. The flow on the inboard side of the body flap close to the hinge line also appears to move forward as it moves off the side. This is also shown in figure 15(b) (alpha = 20°), although the direction of the flow is not as easily seen. The inclined surface of the deflected body flap with the skewed hinge line produced a larger area influenced by the inboard flow off the control (figs. 15(c) and (d)). The corresponding

increase in surface pressure in this region would be expected to enhance the roll effectiveness of the control.

The yaw controller (see fig. 2(e)) produced adequate yawing moments accompanied by small favorable rolling moments (fig. 16). The yaw angular acceleration at Mach 20 is $15.5°/sec^2$ for a controller deflection of 90° as calculated with the inertial data and nominal entry trajectory conditions used in the simulations described in reference 10. Deflection of the controller also produced nose-down pitching-moment coefficients larger than the elevon trim capability. As with the body flaps, the deflected control induces increased pressure on the lower body surface ahead of and to the outboard side of the controller. This is indicated in the surface oil-flow photographs of figure 17(a) and (b), and is similar to that observed for the shuttle orbiter model of reference 11. The region of high pressure would be expected to produce a sizable adverse rolling moment because of its outboard location, but the data of figure 16 show that the rolling moment is slightly favorable. The side loading on the controller combined with its location below the model center of gravity more than offset the adverse effects of the bottom surface loading. In the case of the orbiter model of reference 11, the side loading on the controller was reinforced by the surface normal loading because of its inboard location relative to the controller.

Although no heating tests have been performed, it is expected (as pointed out in reference 11) that the overall heating of the controller would be high because of its location in the high energy shock layer on the bottom of the model. In addition to high heating on the forward face of the controller, there may possibly be high heating associated with flow behind the deflected controller (fig. 17). This would tend to increase the heating in the cavity from which the controller was deployed.

CONCLUSIONS

An analysis of the data obtained from a control effectiveness study for a 0.0196-scale HL-20 model with fin-mounted elevons, flush-mounted body flaps, and a flush-mounted yaw controller at Mach 10 resulted in the following conclusions:

1. For the given center-of-gravity location of 54 percent of the model reference length, the model was longitudinally and laterally stable throughout the angle-of-attack range tested.
2. The longitudinal control effectiveness of the fin-mounted elevons was minimal. The model could not be trimmed above an angle of attack of 23.5°, which is less than the 30° angle of attack prescribed for the entry trajectory.
3. The conventional flush-mounted body flap was effective in roll; however, deflection of the control for roll resulted in adverse yawing moments. Skewing the body-flap hinge line 25° eliminated the adverse yawing moments without materially affecting the roll effectiveness.
4. The flush-mounted yaw controller was effective in yaw and produced a small favorable rolling moment.
5. Deflection of the body flap or yaw controller resulted in negative pitching moment coefficients of -0.009 and -0.006 respectively, which increased the existing deficit in longitudinal trim capability.

REFERENCES

1. Stone, H. W. and Piland, W. M.: 21st Space Transportation System Design Approach: HL-20 Personnel Launch System. AIAA Journal of Spacecraft and Rockets, Vol. 30, No. 5, pp. 521-528, September, 1993.
2. Ware, G. M.; Spencer, B. Jr.; and Micol, J. R.: Aerodynamic Characteristics of Proposed Assured Crew Return Capability (ACRC) Lifting Body Configuration. AIAA-89-2172, July 1989.
3. Cruz, C. I.; Ware, G. M.; Grafton, S. B.; Woods, W. C.; and Young, J. C.: Aerodynamic Characteristics of a Proposed Personnel Launch System (PLS) Lifting Body Configuration at Mach Numbers from 0.05 to 20.3. NASA TM 101641, November 1989.
4. Micol, J. R.: Experimental and Predicted Aerodynamic Characteristics of a Proposed Assured Crew Return Vehicle (ACRV) Lifting Body Configuration at Mach 6 and 10. AIAA 90-1403, June 1990.
5. Ware, George M. and Cruz, Christopher I.: Aerodynamic Characteristics of the HL-20. AIAA Journal of Spacecraft and Rockets, Vol. 30, No. 5, pp. 529-536, September-October, 1993.
6. Ware, G. M.: Transonic Aerodynamic Characteristics of a Proposed Assured Crew Return Capability (ACRC) Lifting Body Configuration. NASA TM 4117, June 1989.
7. Ware, G. M.: Supersonic Aerodynamic Characteristics of a Proposed Assured Crew Return Capability (ACRC) Lifting Body Configuration. NASA TM 4136, November 1989.
8. Cruz, Christopher I. and Ware, George M.: Control Effectiveness and Tip-Fin Dihedral Effects for the HL-20 Lifting-Body Configuration at M = 1.6 to 4.5. NASA TM 4697, December 1995.
9. Ware, George M. and Cruz, Christopher I.: Subsonic Aerodynamic Characteristics of the HL-20 Lifting-Body Configuration. NASA TM 4515,   October 1993.
10. Powell, R. W.: Six-Degree-of-Freedom Guidance and Control Analysis of the HL-20. AIAA Journal of Spacecraft and Rockets, Vol. 30, No. 5, pp. 537-542, September 1993.
11. Scallion, W. I.: Performance of an Aerodynamic Yaw Controller Mounted on the Space Shuttle Orbiter Body Flap at Mach 10. NASA TM 109179, February 1995.
12. Miller, C. G. III: Hypersonic Aerodynamic/Aerothermodynamic Testing Capabilities at Langley Research Center. AIAA-92-3937, July 1992.
13. Spencer, B. Jr.; Fox, C. H. Jr.; and Huffman, J. K.: A Study to Determine Methods of Improving the Subsonic Performance of a Proposed Personnel Launch System (PLS) Concept. NASA TM 110201, December 1995.
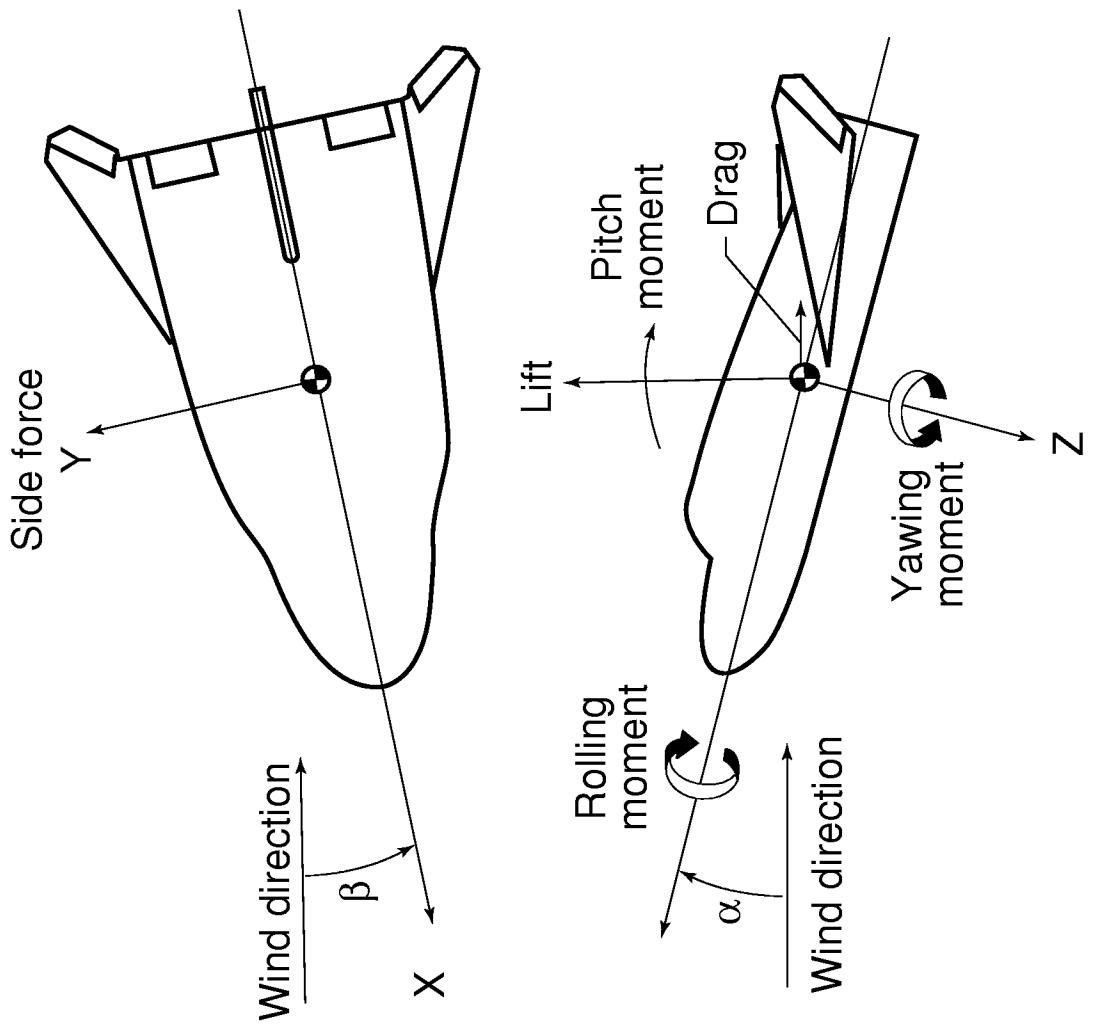
Figure 1. System of axes, showing the positive direction of forces, moments and angles.

Yaw controller

30°

End View

2.826

1.25°

Plan View

Bottom View

HL

HL

6.6° Body
Flap

3.117

5.772

Side View
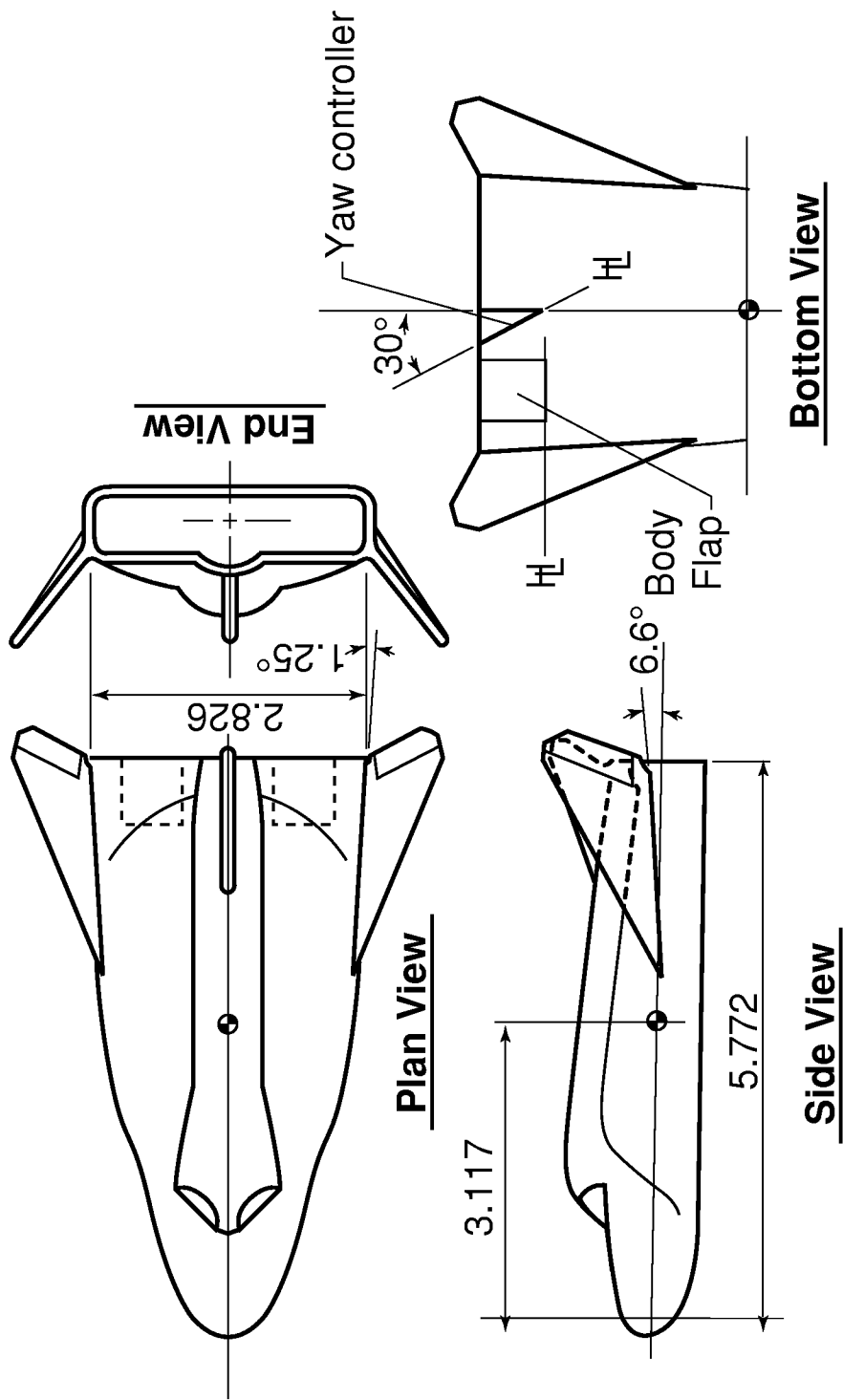
(a) General arrangement of the configuration.

Figure 2. Sketches of the model and controls. All dimensions are given in inches.

(b) Tip fin details.

Figure 2. Continued.

12

.700

.500

.050

0°

-10°

-20°

10°

20°

Elevon Brackets

Right elevon

.250

.804

1.047

.243

.295

.125

.110

.15 .400 .15 .300

1.162

Left elevon

Elevon Plan
Thickness = 0.10
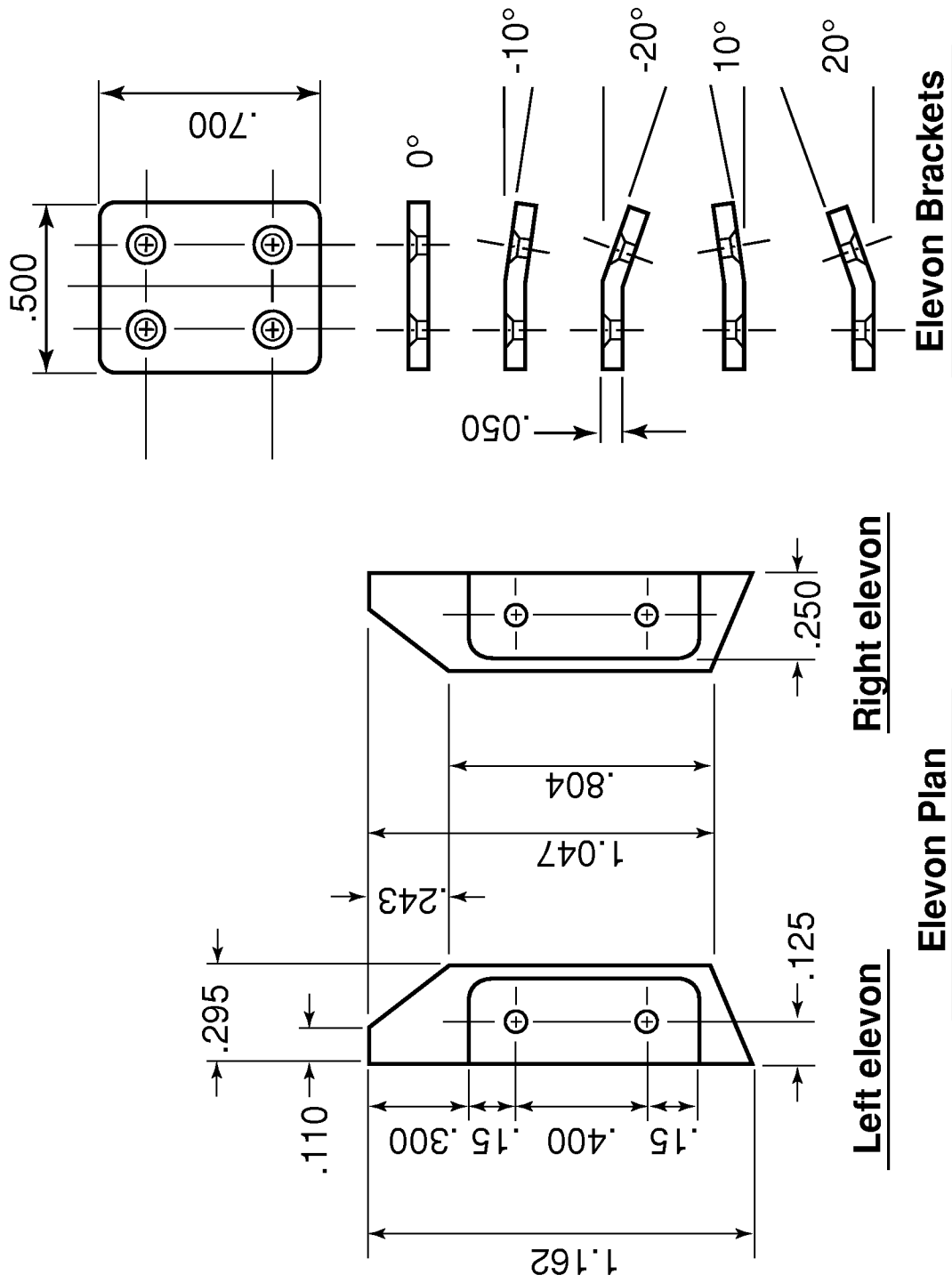
(c) Sketches of elevons and deflection brackets.

Figure 2. Continued.

Skewed-Hinge-Line Body Flap
Left-Hand Control

Auxiliary View

15° & 30°

.640
.400
.120
.194
.477
.125
.12R
25°

30° Flap
15° Flap

3-D View

Body Flaps

.640
.400
.120
.050
.671
.421
.250
.125
10°
20°
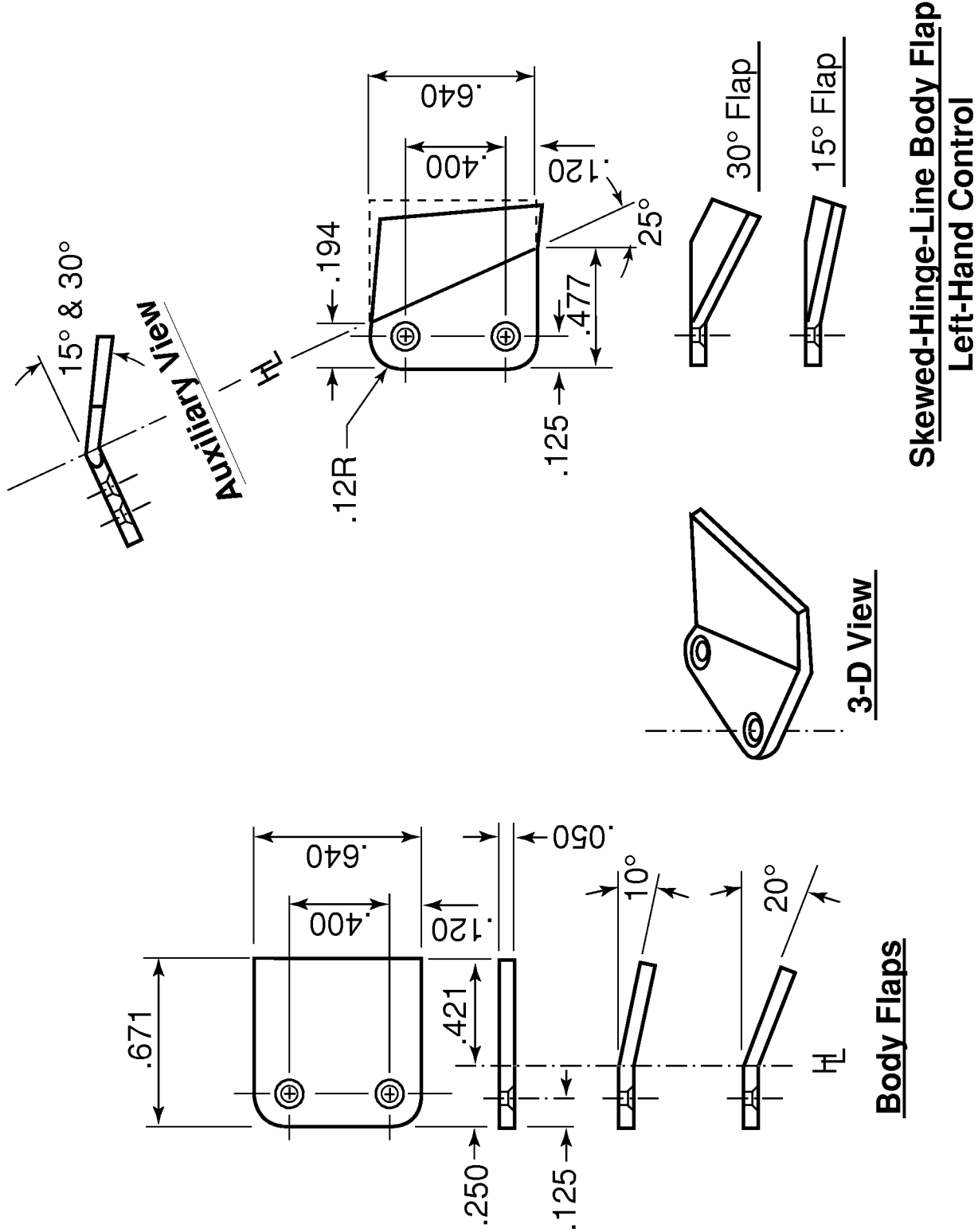
(d) Lower surface body flaps.

Figure 2. Continued.

Cover Plate
Thickness = .040

90° Yaw Control
Left Hand Side

45° Yaw Control
Left Hand Side

90° Control

45° Control

3-D View
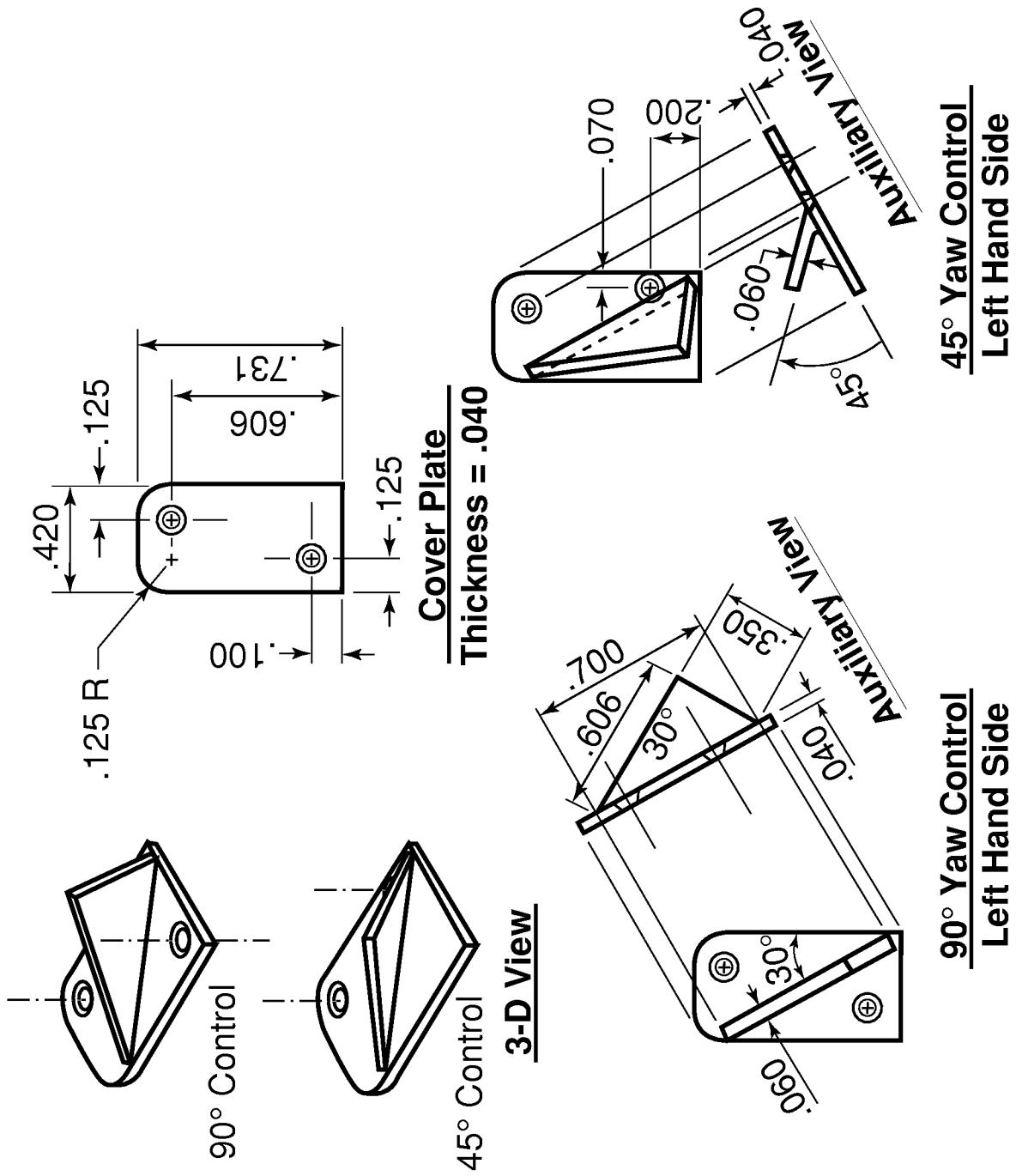
(e) Lower surface yaw controllers.

Figure 2. Concluded.

15
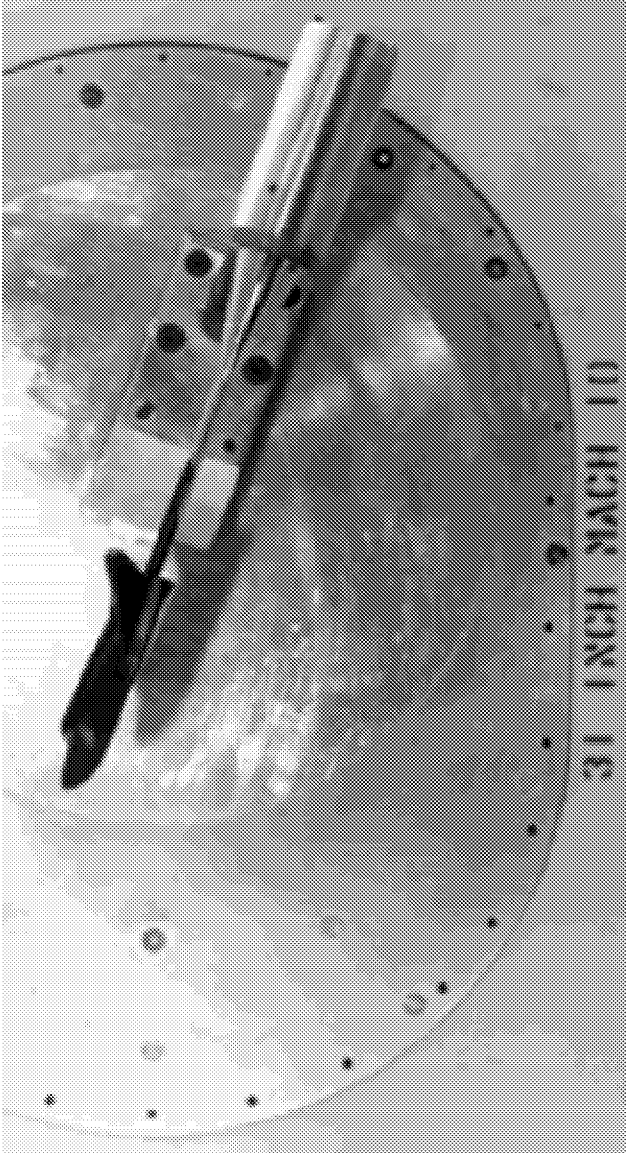
(a) Model mounted for test in the 31 Inch Mach 10 Tunnel.

Figure 3. Photographs of the 0.0196-scale HL-20 model and components, and full-scale mock-up.
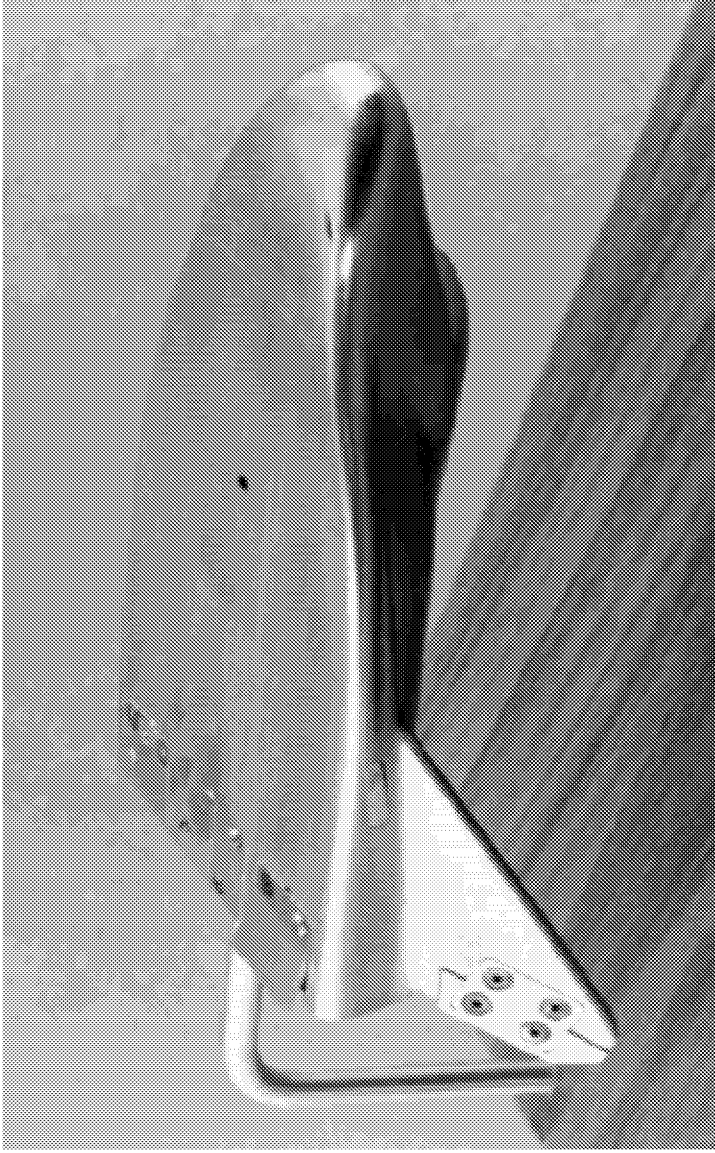
(b) Model with conventionally-hinged body flap at 10° deflection.

Figure 3. Continued.
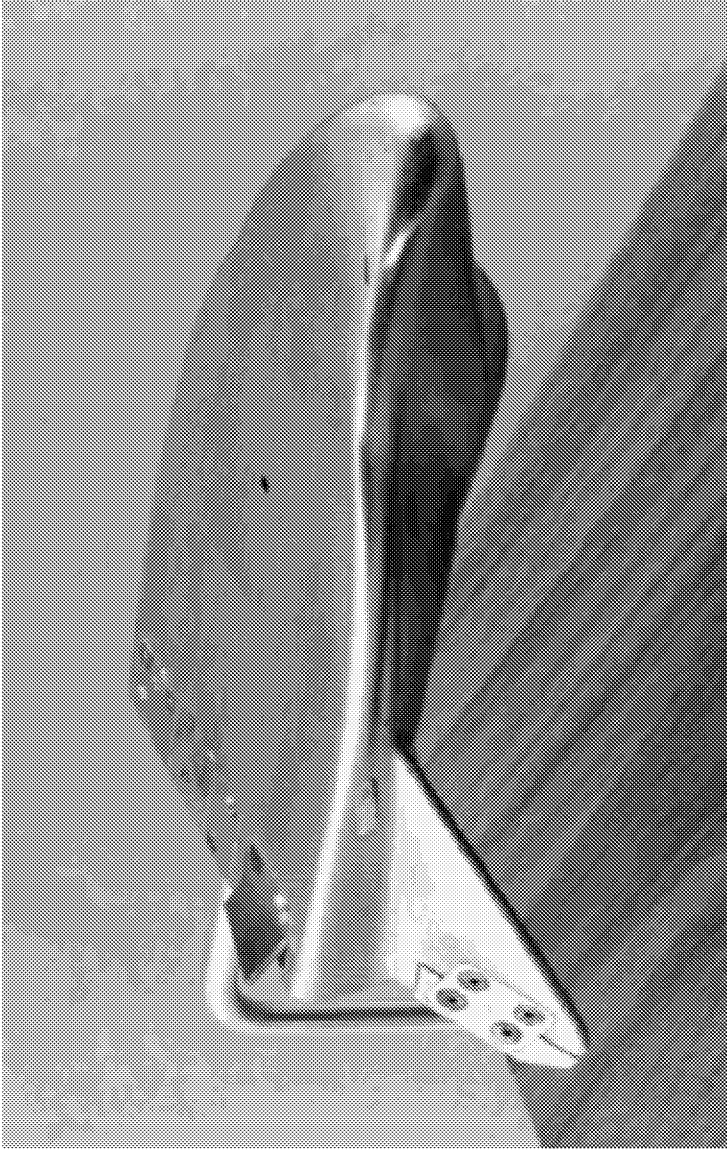
(c) Model with body flap hinge line skewed 25° at 15° deflection.

Figure 3. Continued.
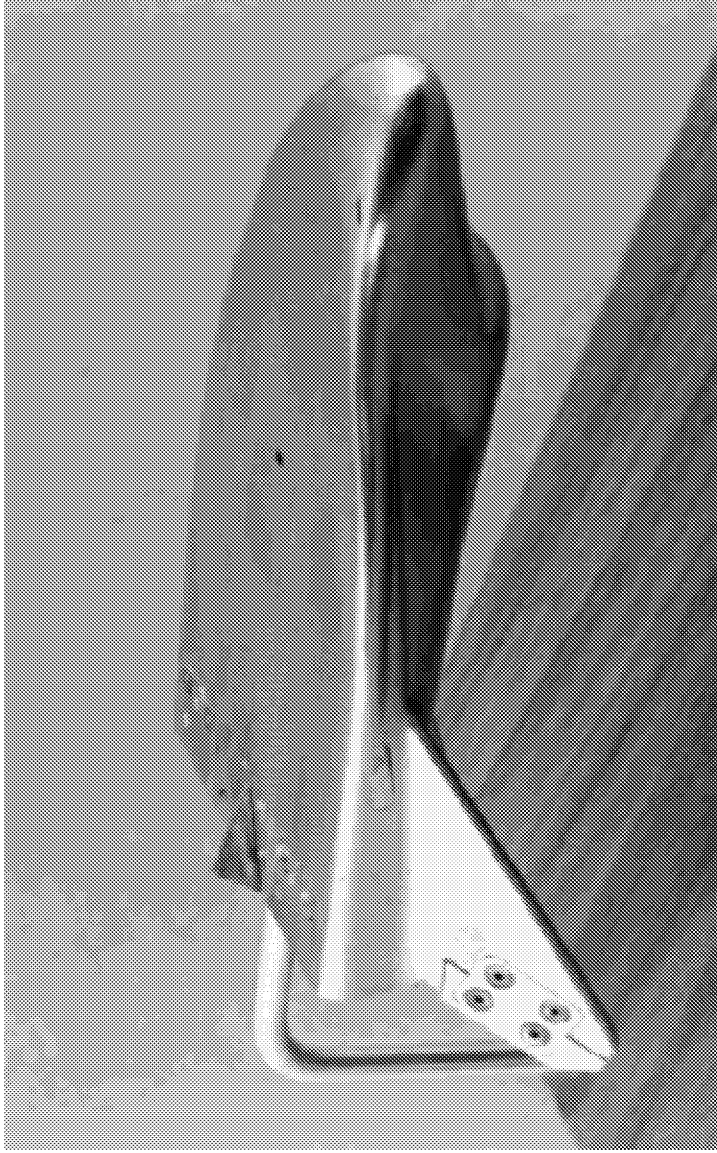
(d) Model with left-hand yaw controller deflected 90°.

Figure 3. Continued.
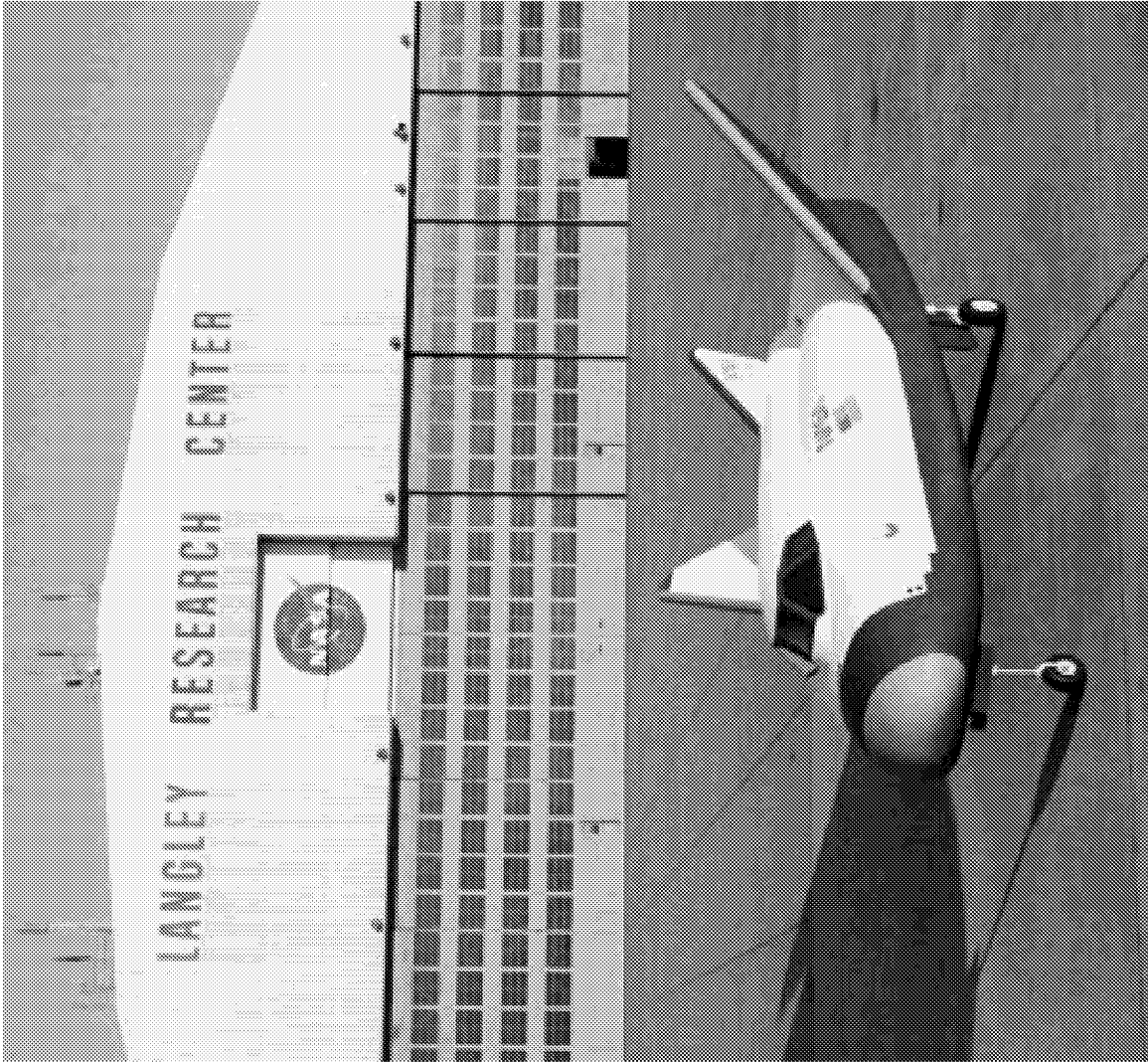
(e) Full-scale mock-up of the HL-20.

Figure 3. Concluded.
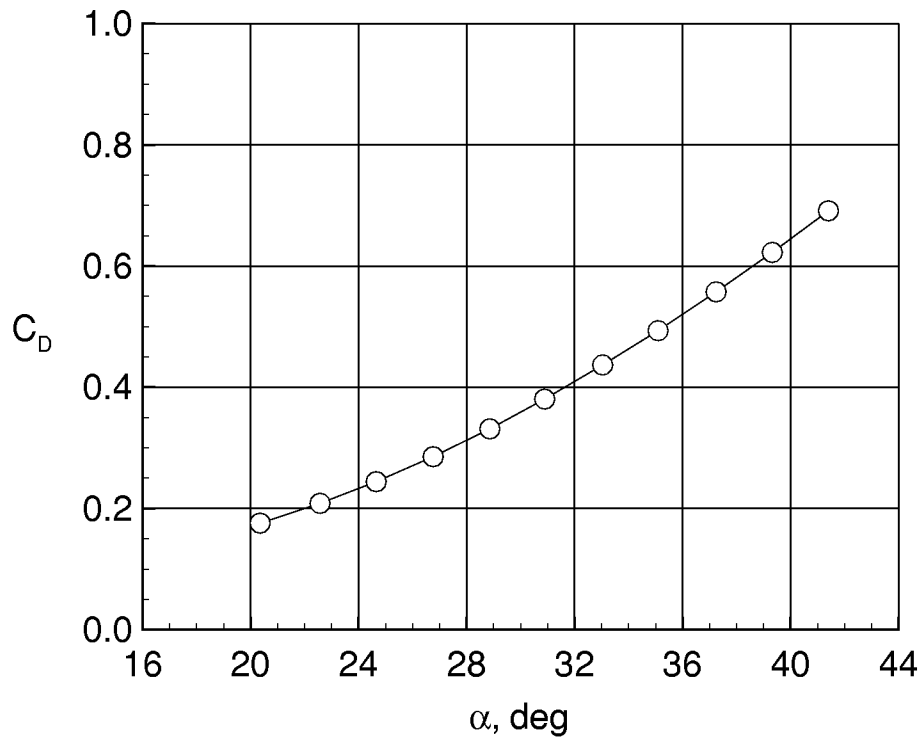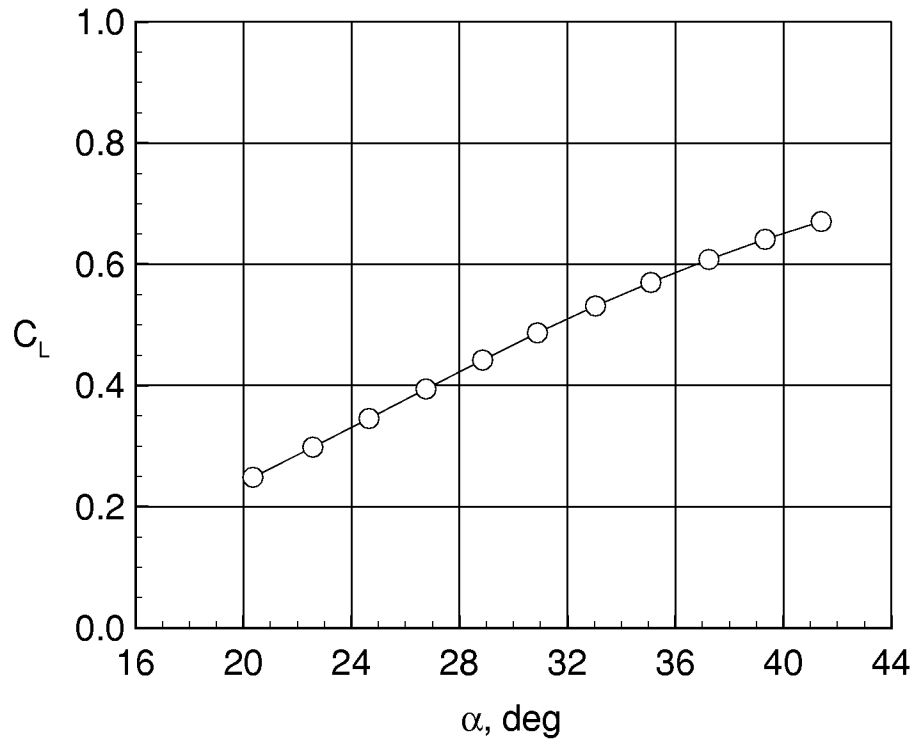
(a) C_L and C_D versus angle of attack.

Figure 4.- longitudinal characteristics of the basic HL-20 model.
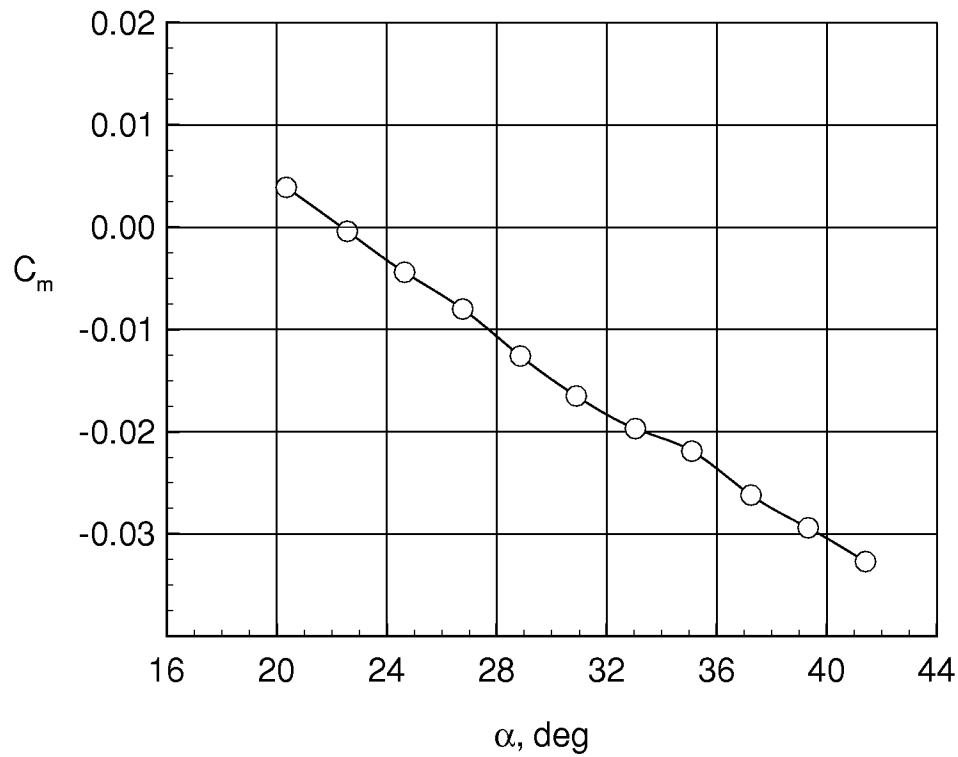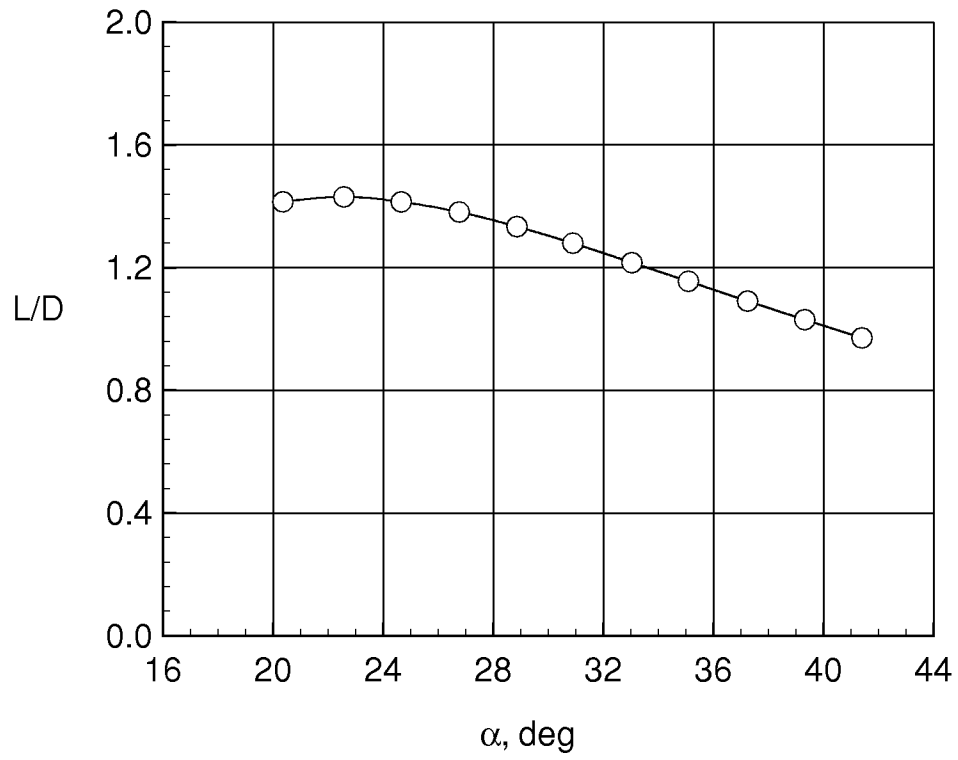
(b) L/D and C_m versus alpha.

Figure 4.-Continued.
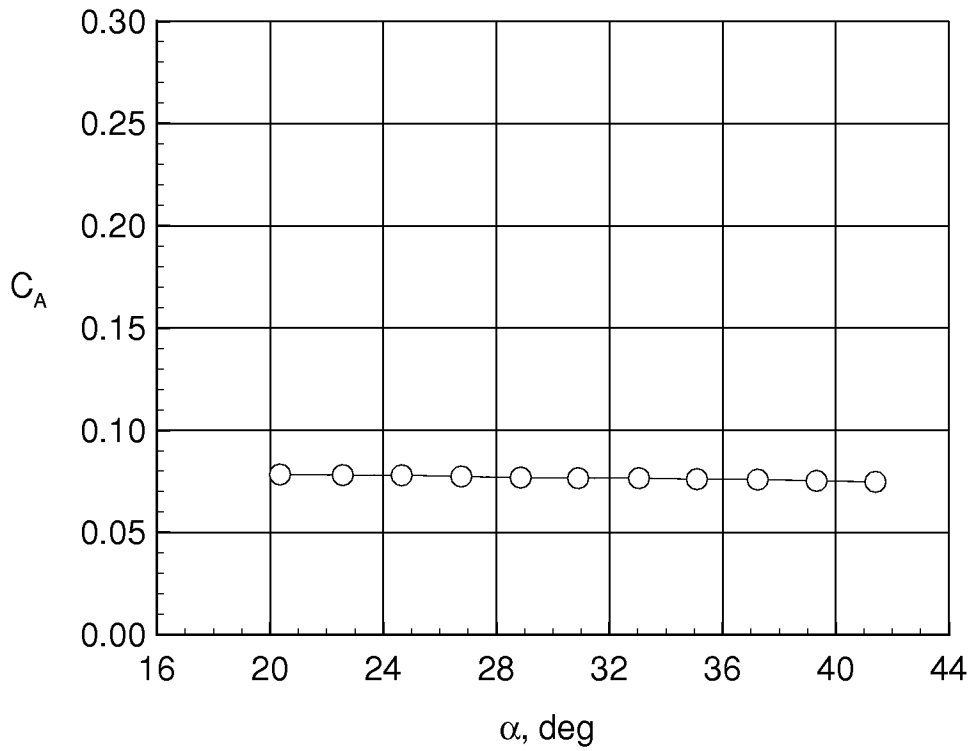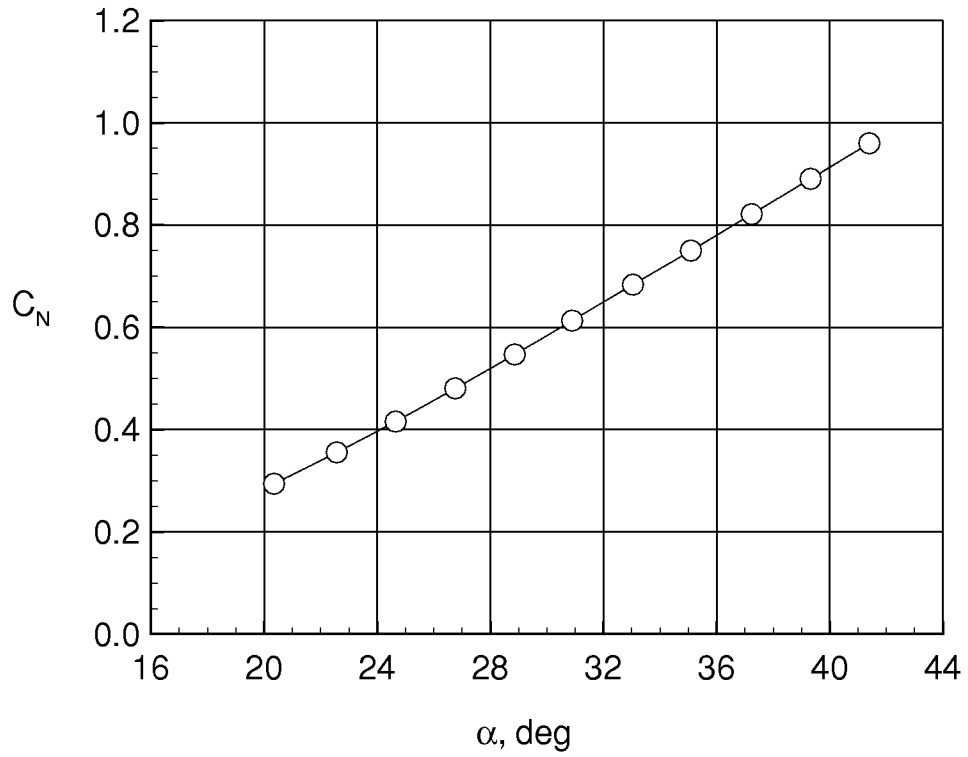
(c) C_N and C_A versus angle of attack.

Figure 4.-Concluded.
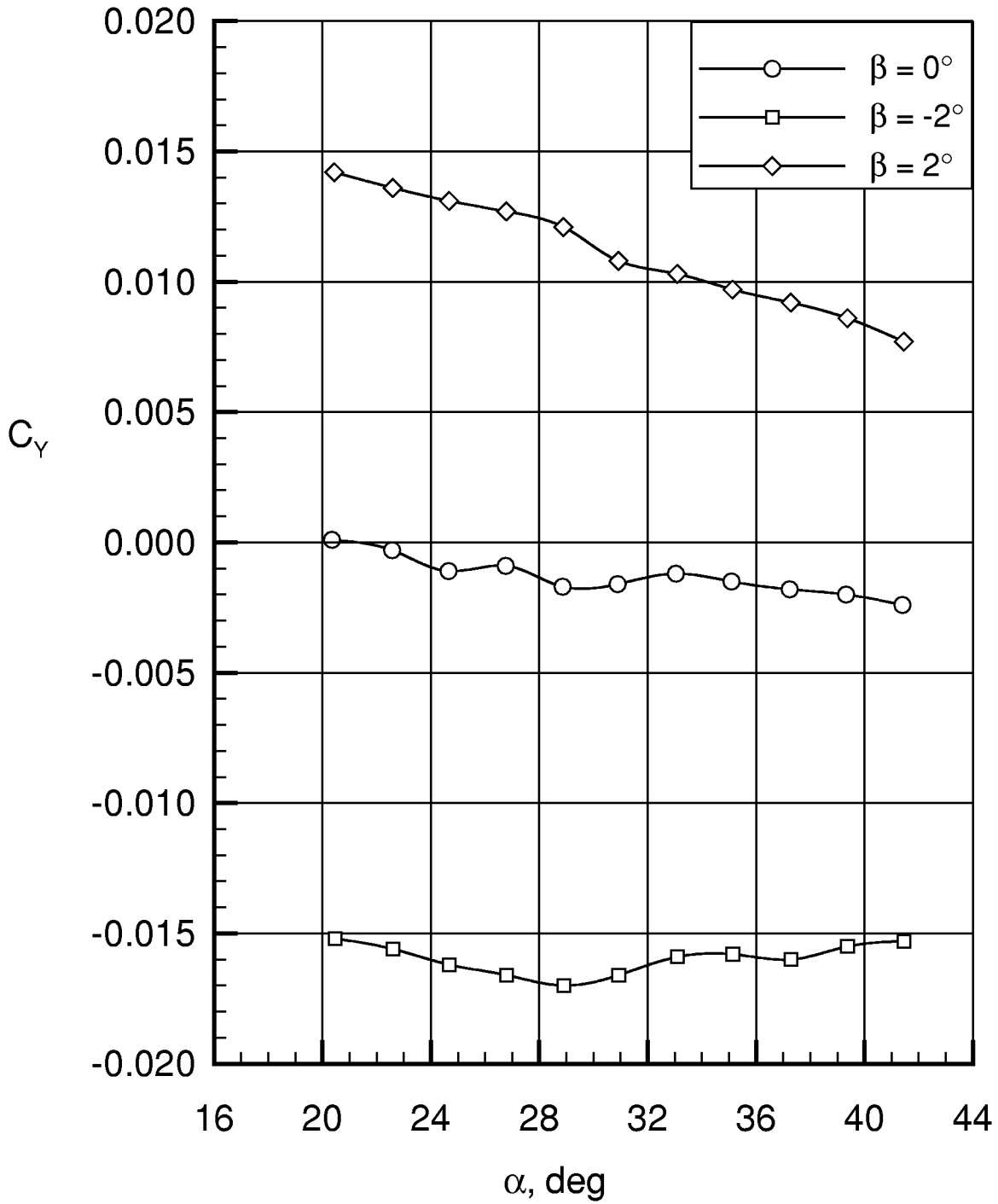
(a) C_Y versus angle of attack.

Figure 5.- Lateral-directional characteristics of the HL-20 model.
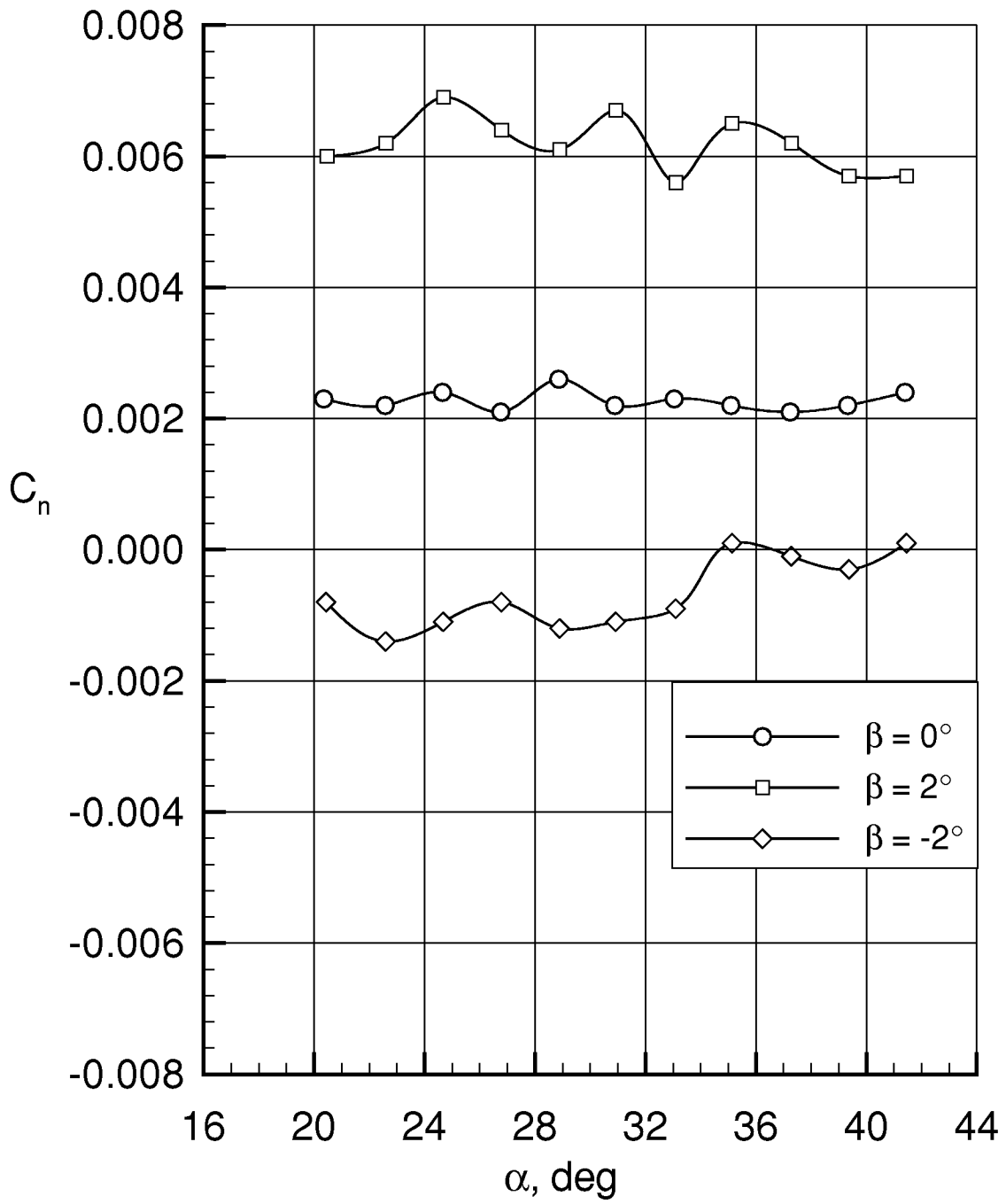
(b) C_n versus angle of attack.

Figure 5.- Continued.
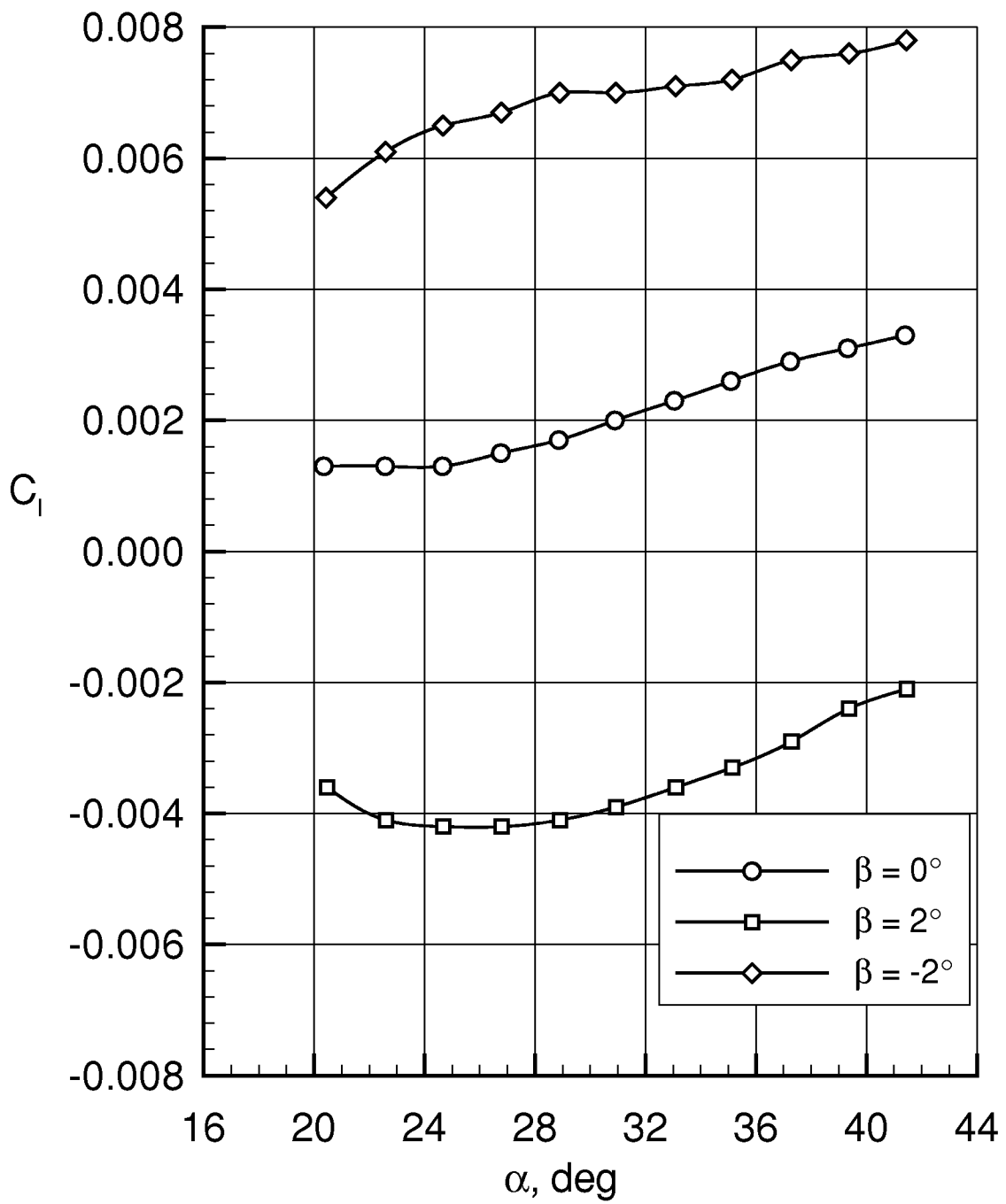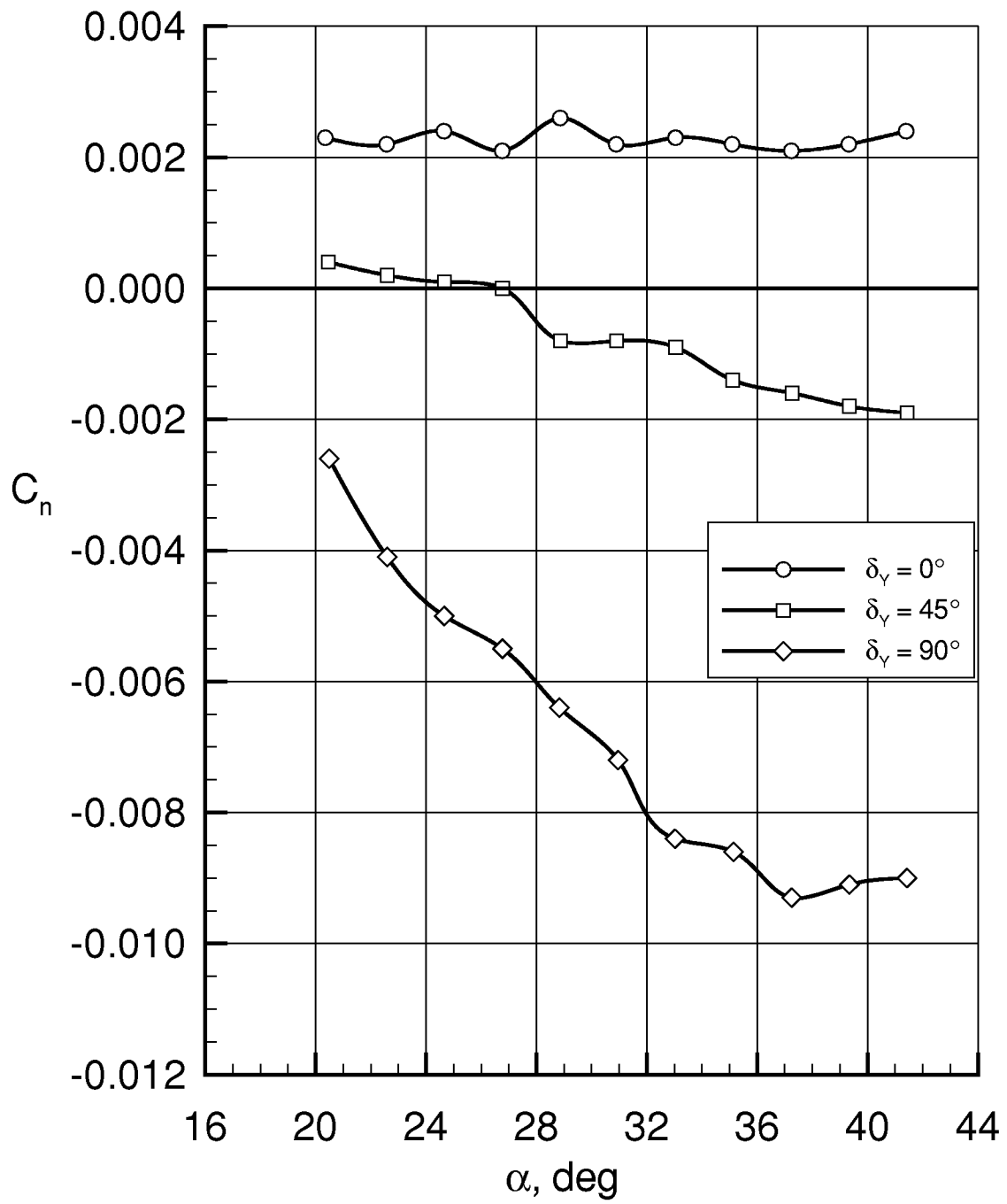
(c) C_l versus angle of attack.

Figure 5.- Concluded.
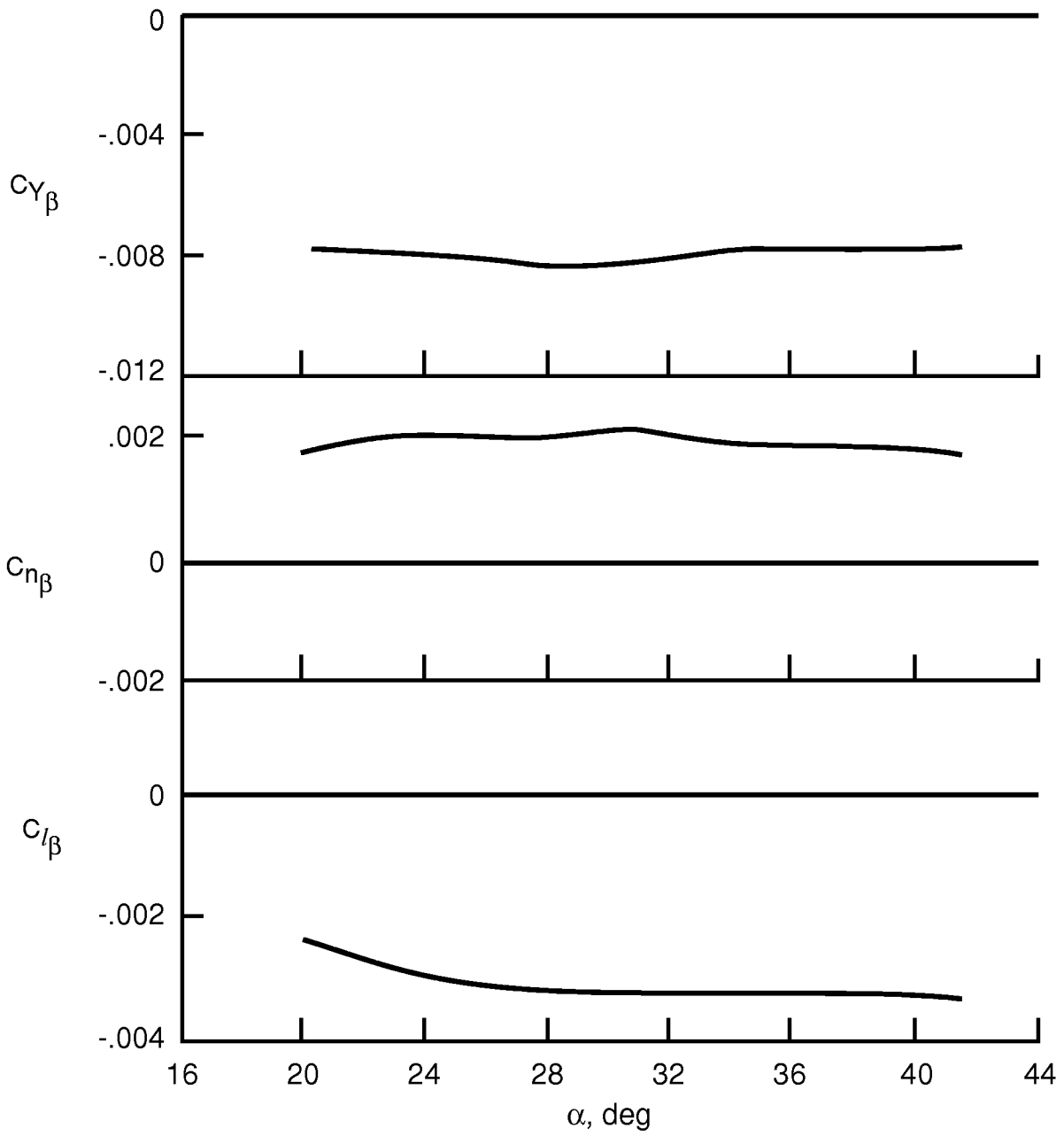
Figure 6. Lateral-directional derivatives versus angle of attack for the HL-20 model with zero control deflections.
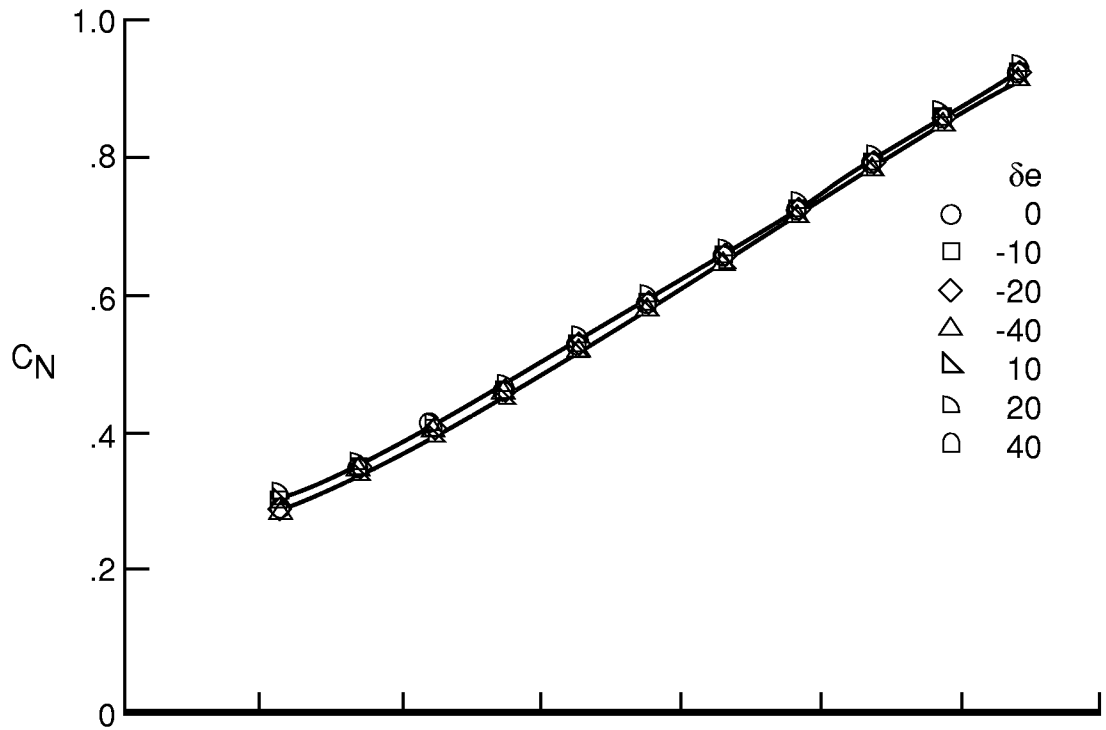
(a) Normal force coefficient.
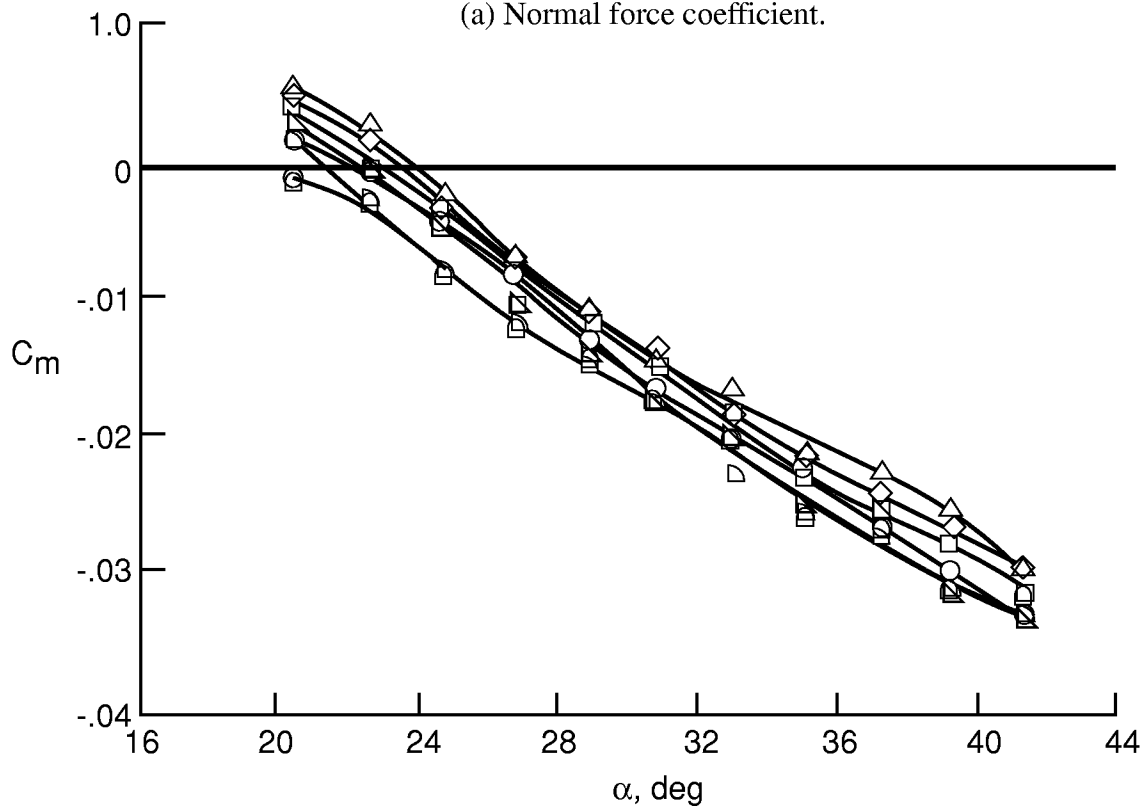
(b) Pitching-moment coefficient.

Figure 7. Effect of elevon deflection on longitudinal characteristics.
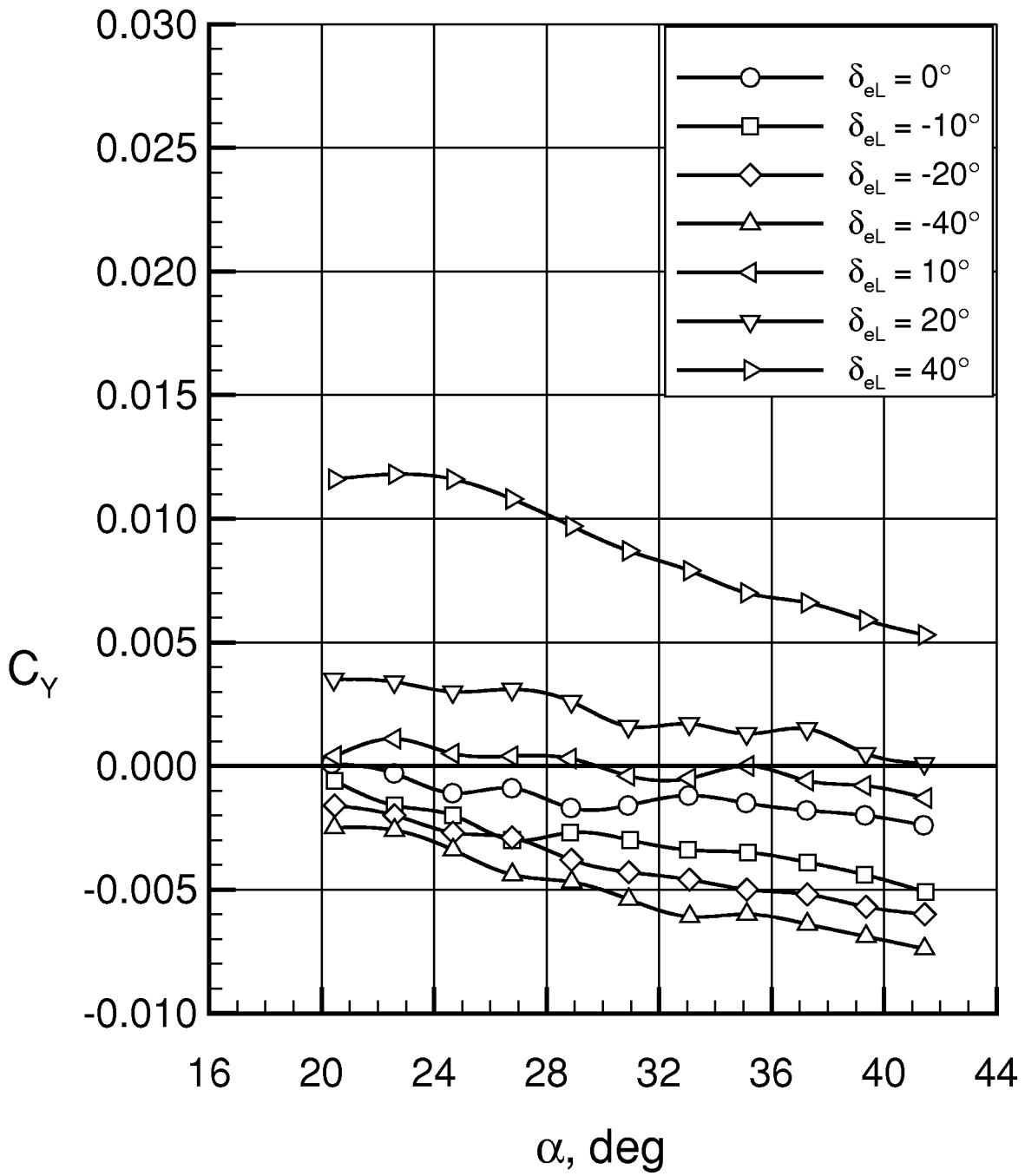
(a) C_Y versus angle of attack.

Figure 8.- Effect of left elevon deflection on the lateral characteristics of the model.
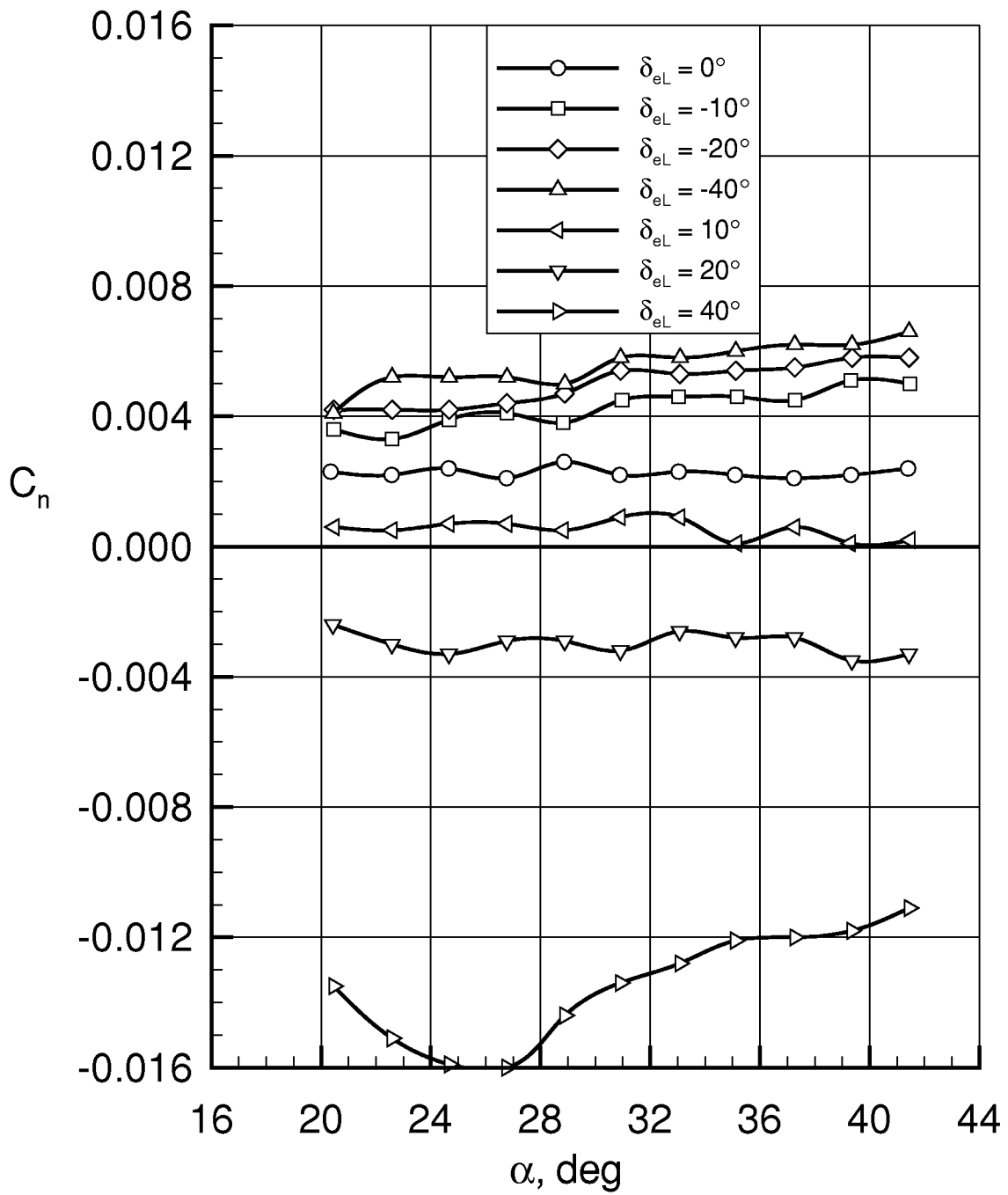
(b) C_n versus angle of attack.

Figure 8.- Continued.
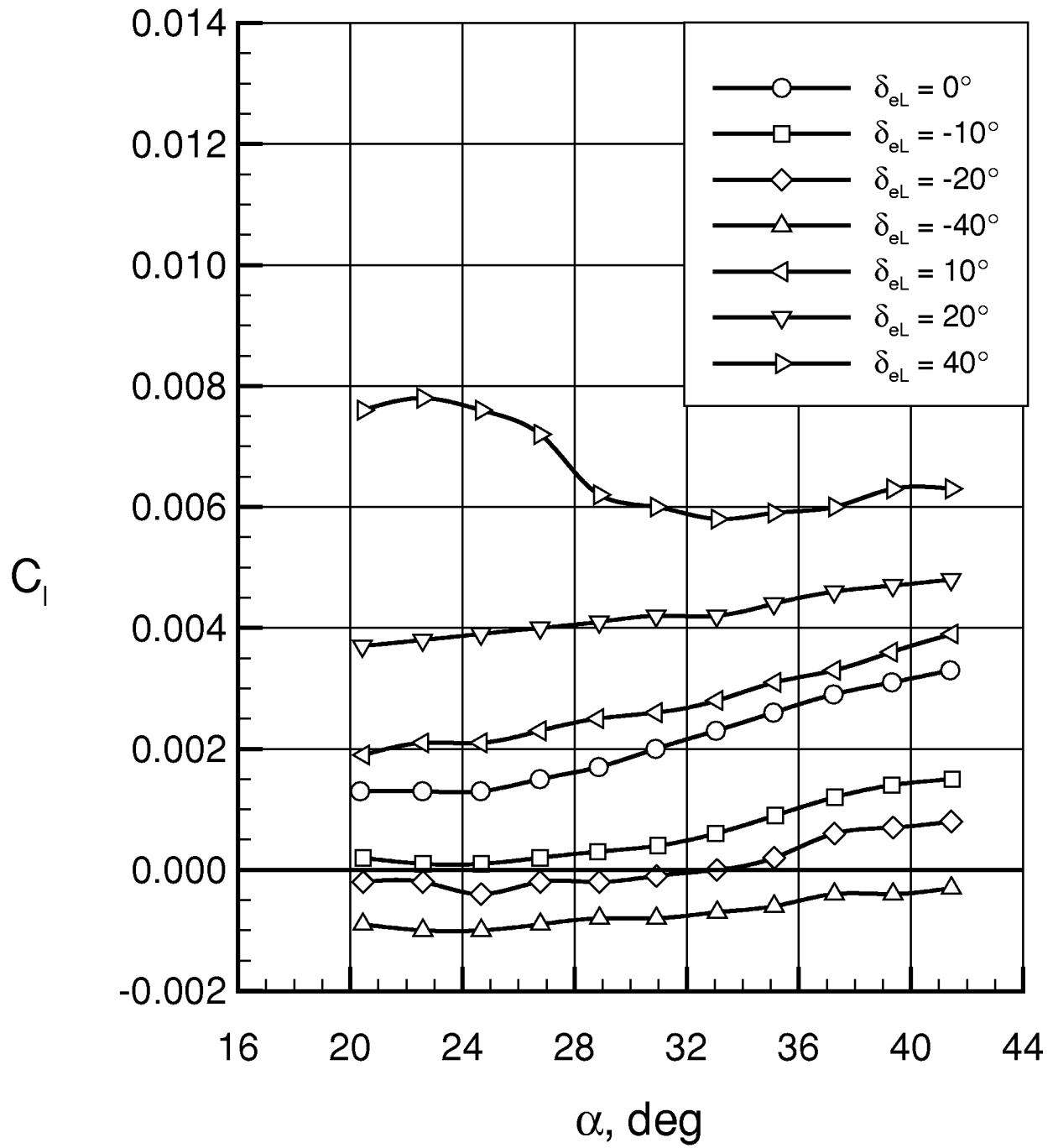
(c) C_l versus angle of attack.

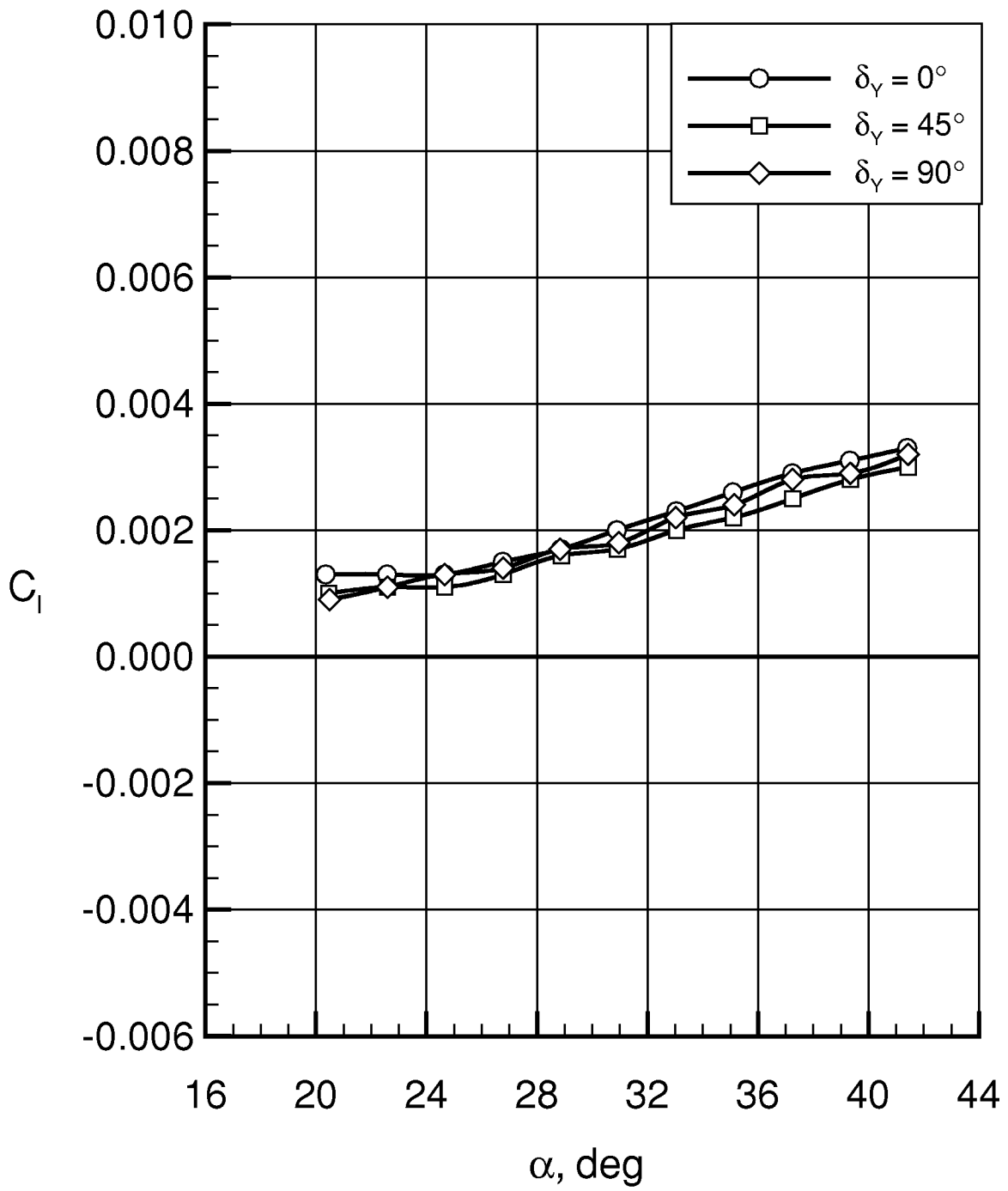Figure 8.- Concluded.
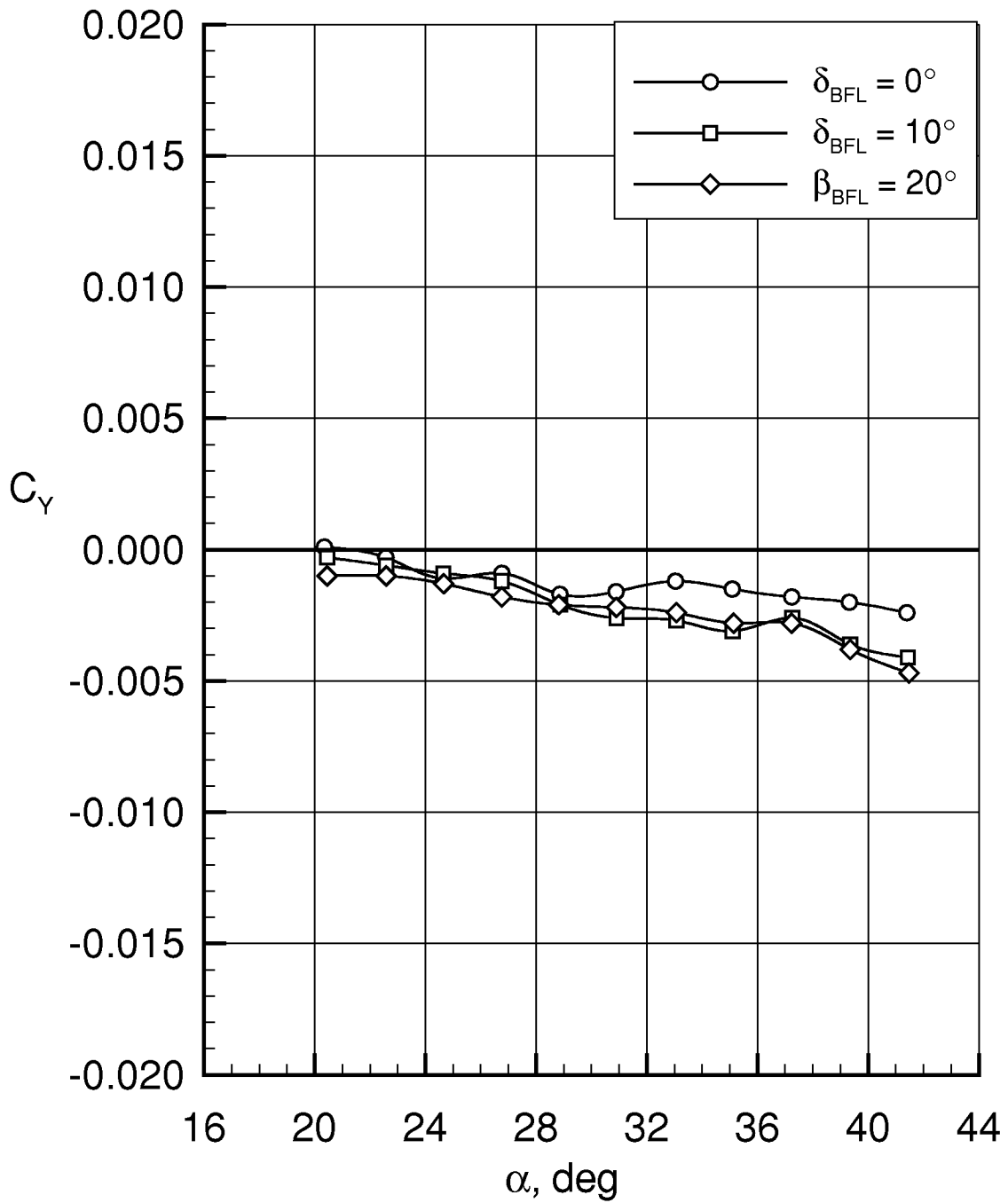
(a) C_Y versus angle of attack

Figure 9.- Effect of body flap deflection on the lateral
and longitudinal characteristics of the model.
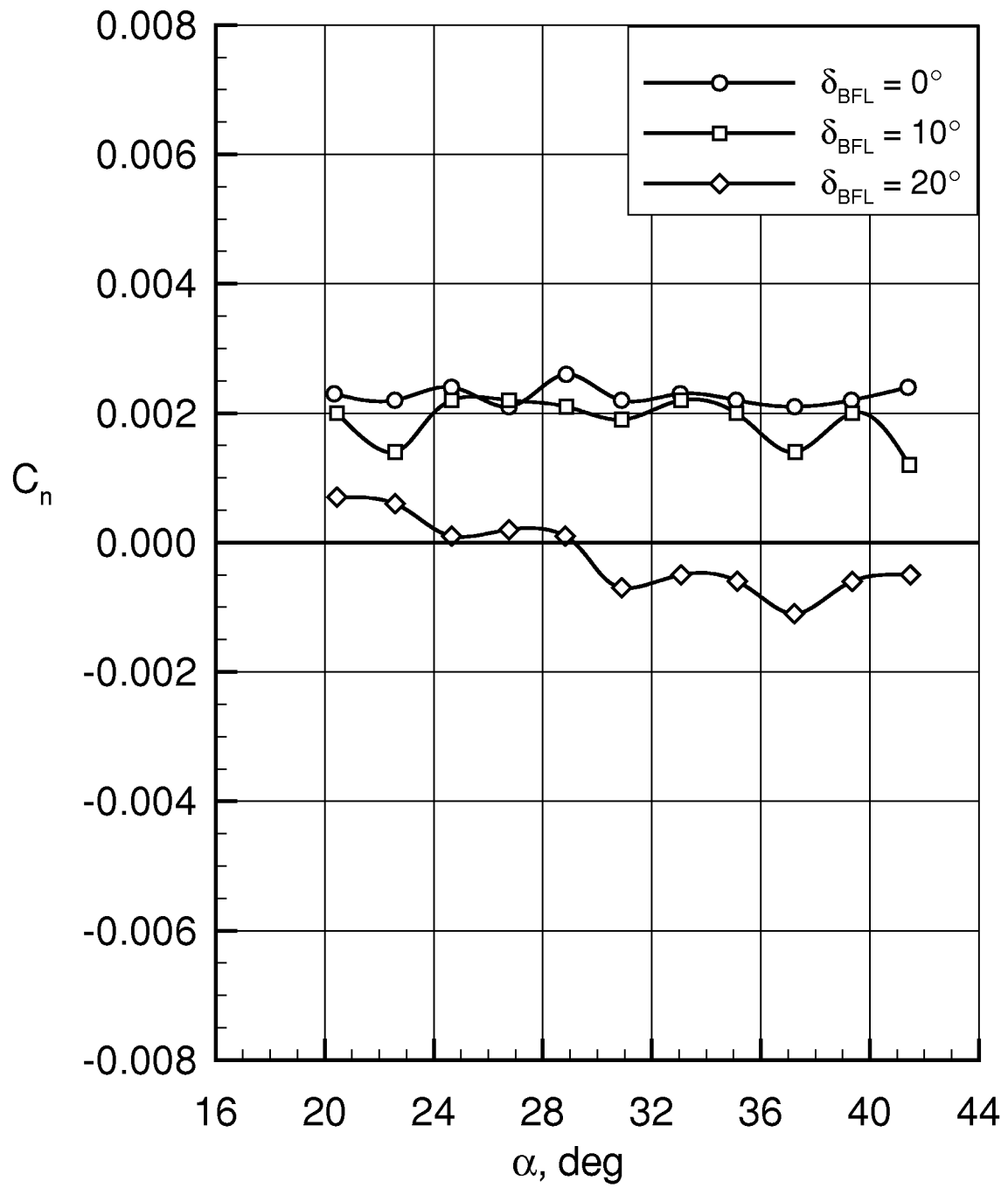
(b) C_n versus angle of attack.
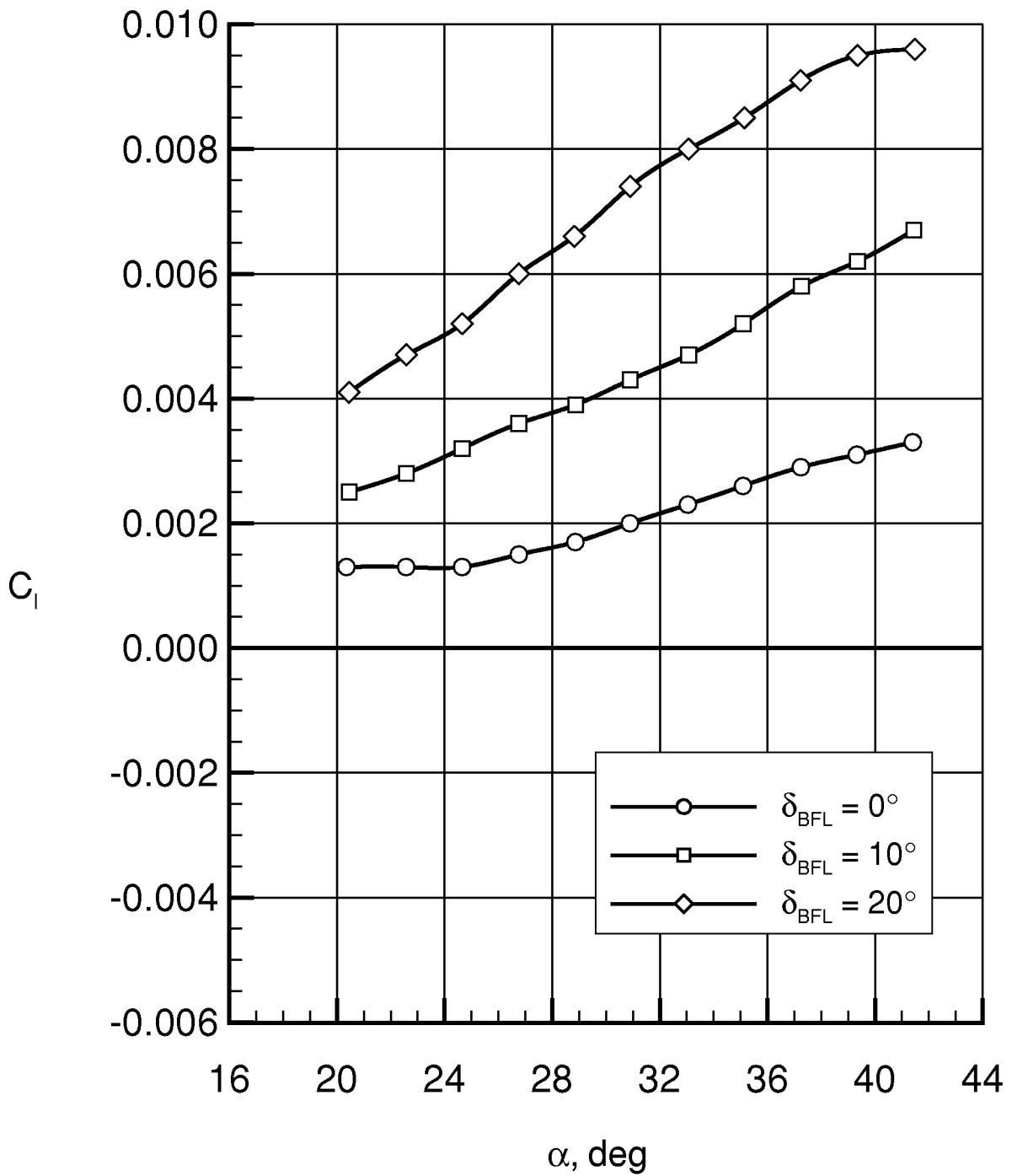
Figure 9.- Continued.

(c) C_l versus angle of attack.
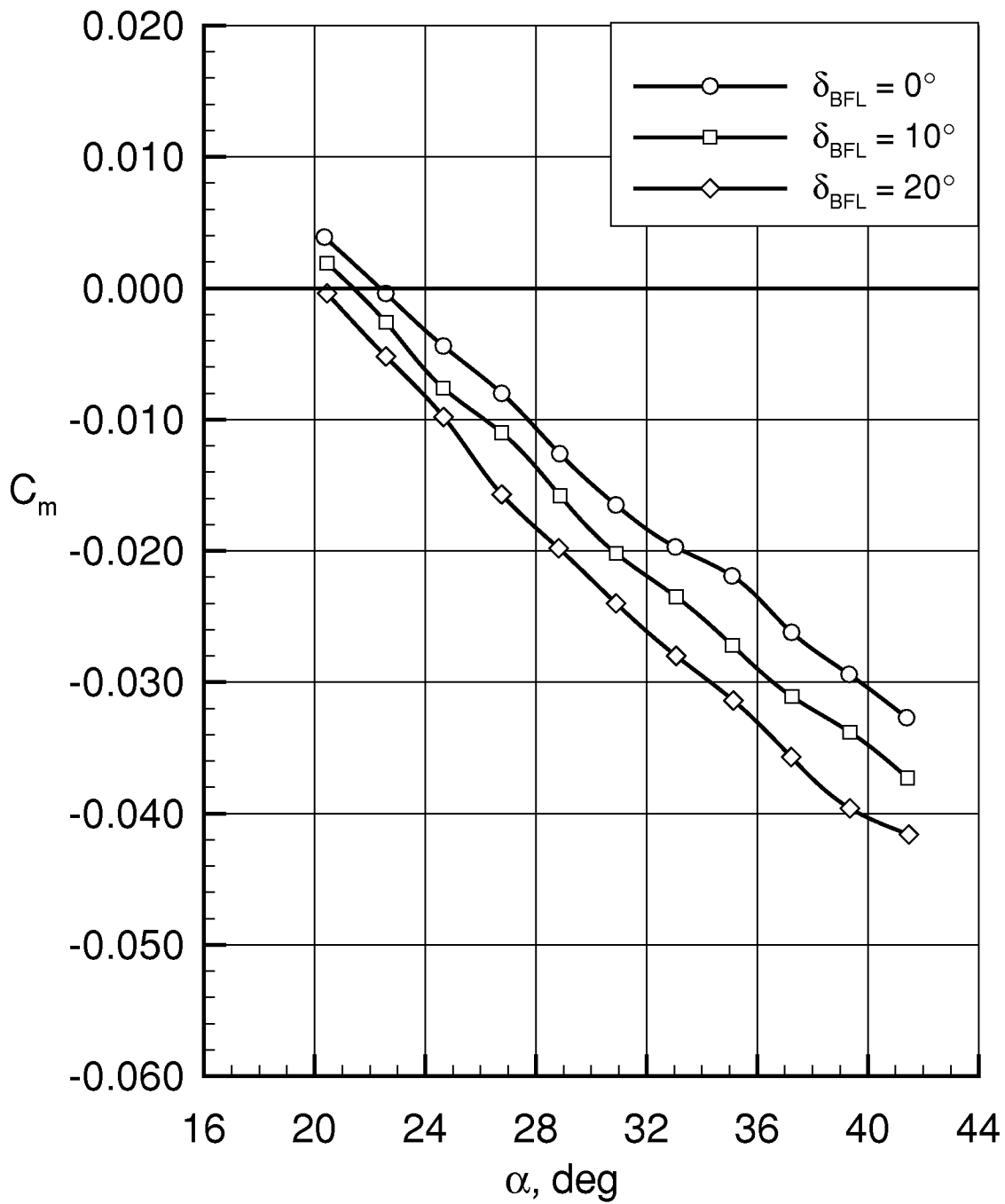
Figure 9.- Continued.

(d) C_m versus angle of attack.

Figure 9.- Concluded.
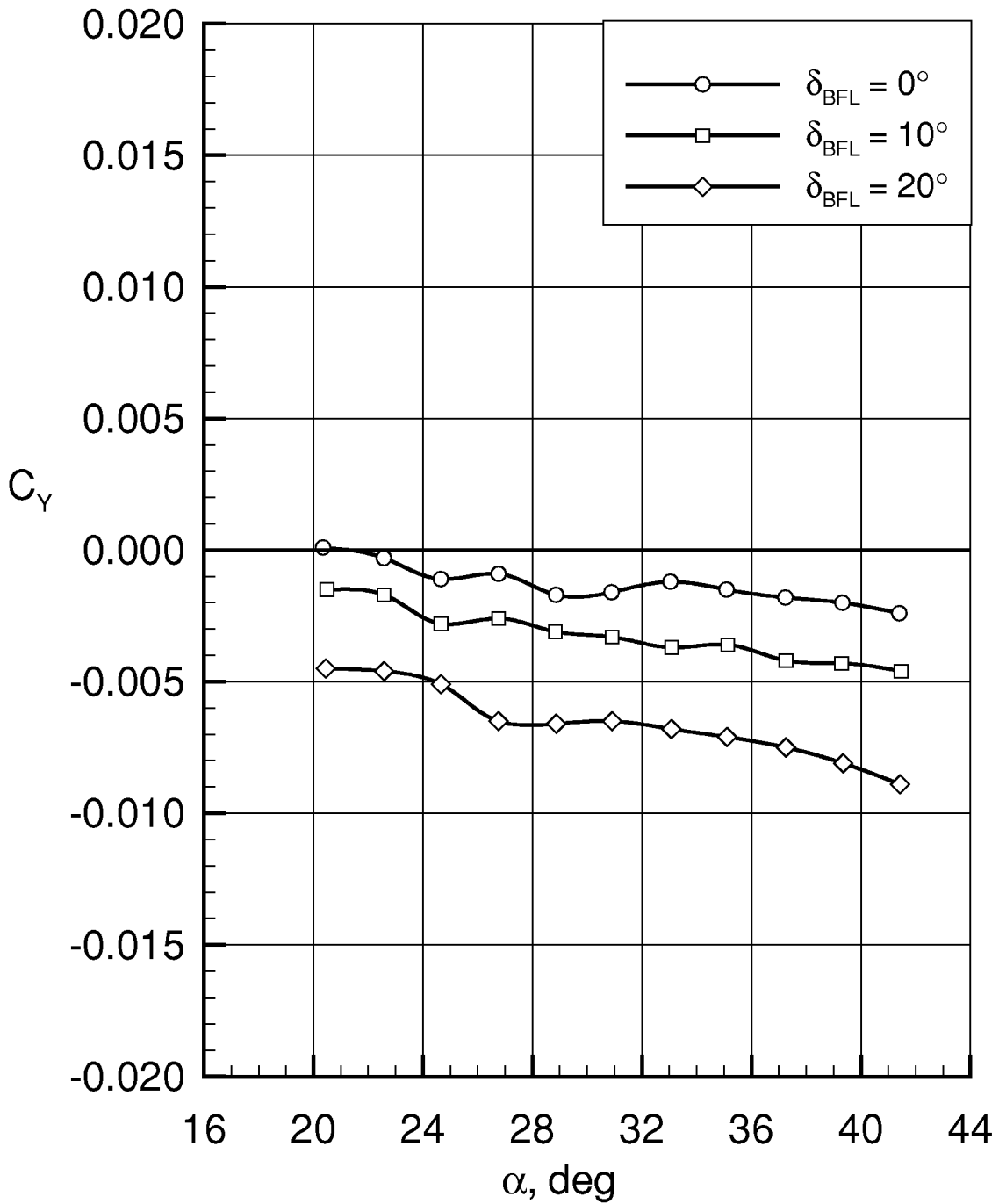
(a) C_Y versus angle of attack.

Figure 10.- Effect of skewed-hinge body flap deflection on lateral and longitudinal characteristics of the model.
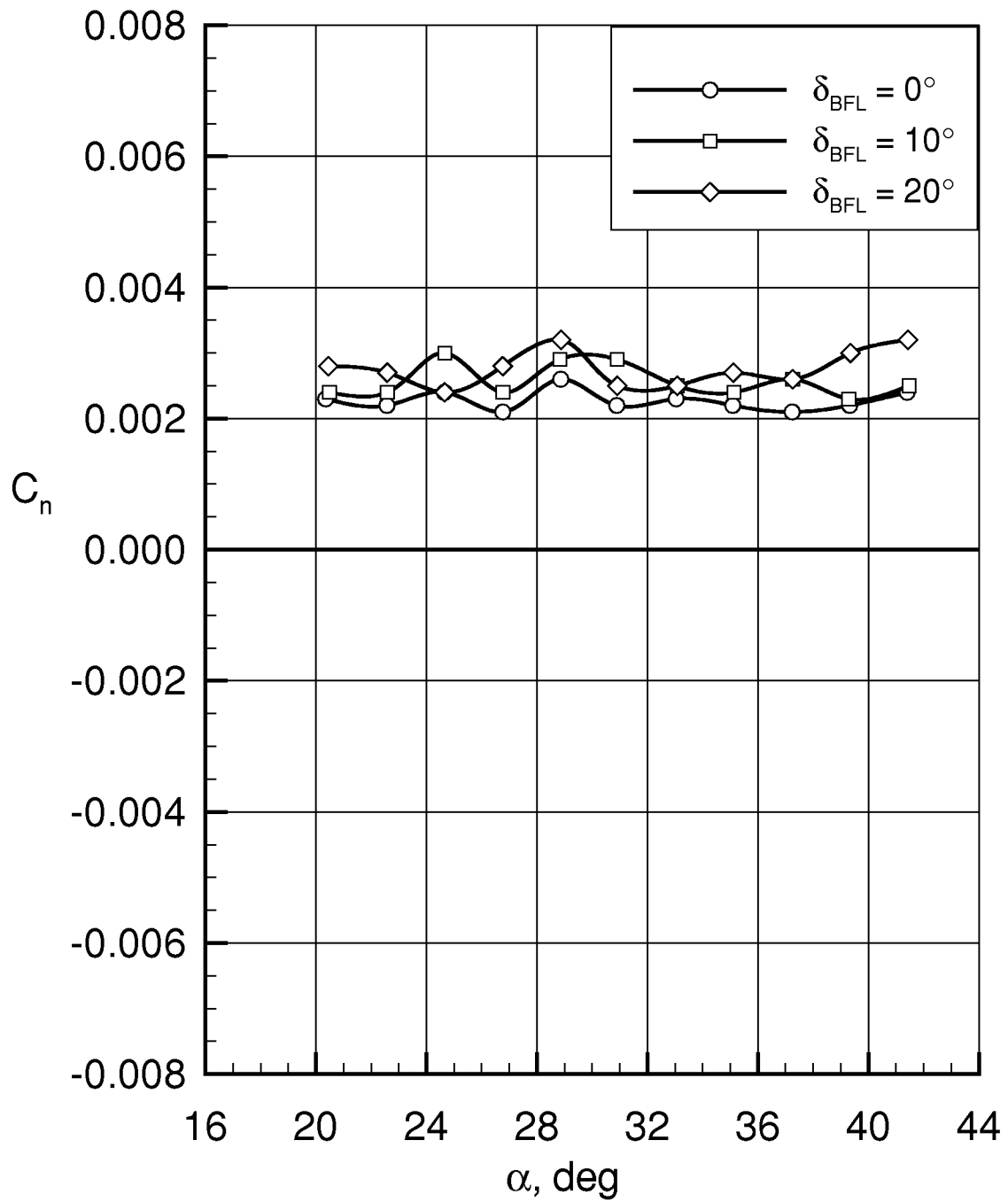
(b) C_n versus angle of attack.

Figure 10.- Continued.
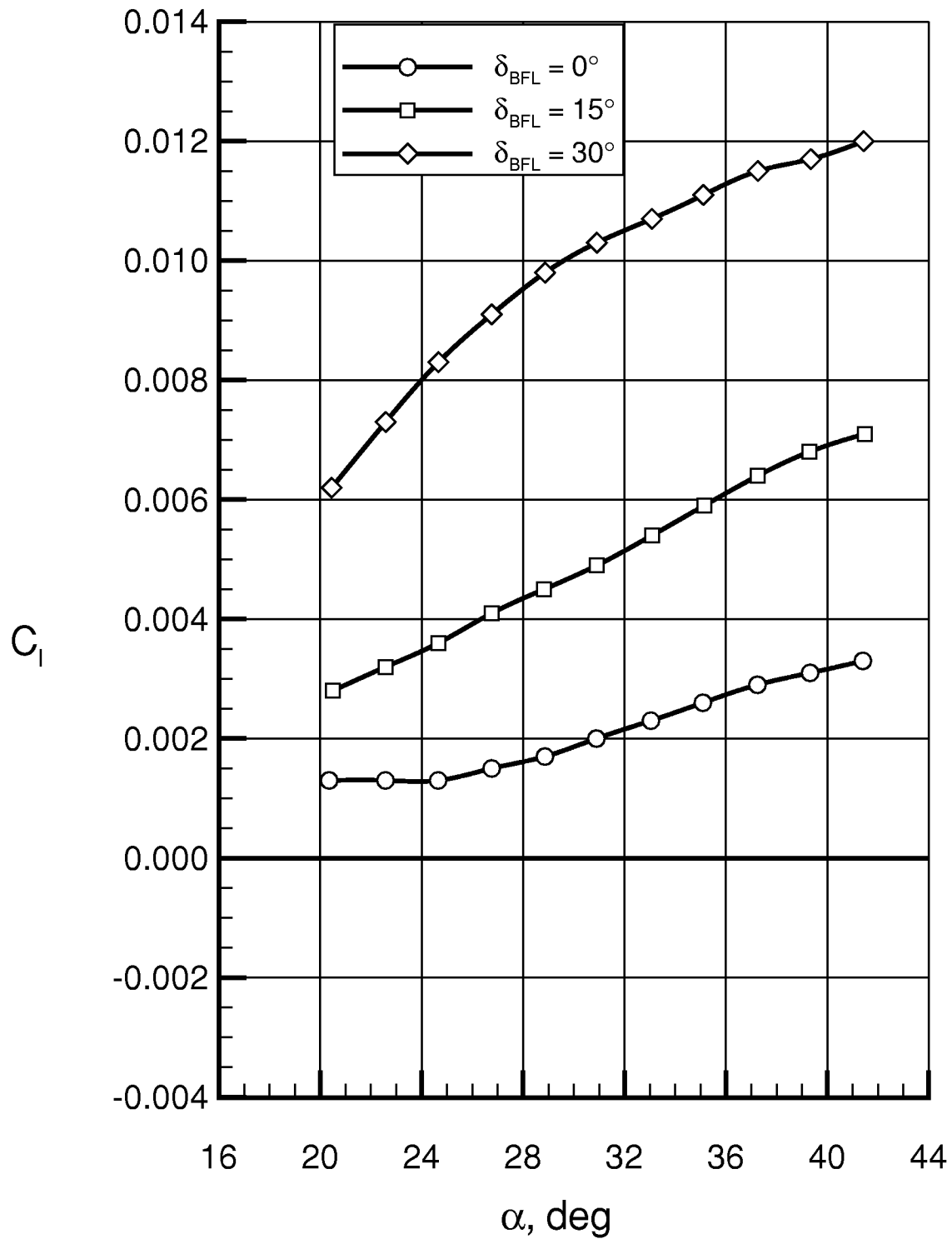
(c) C_l versus angle of attack.

Figure 10.- Continued.
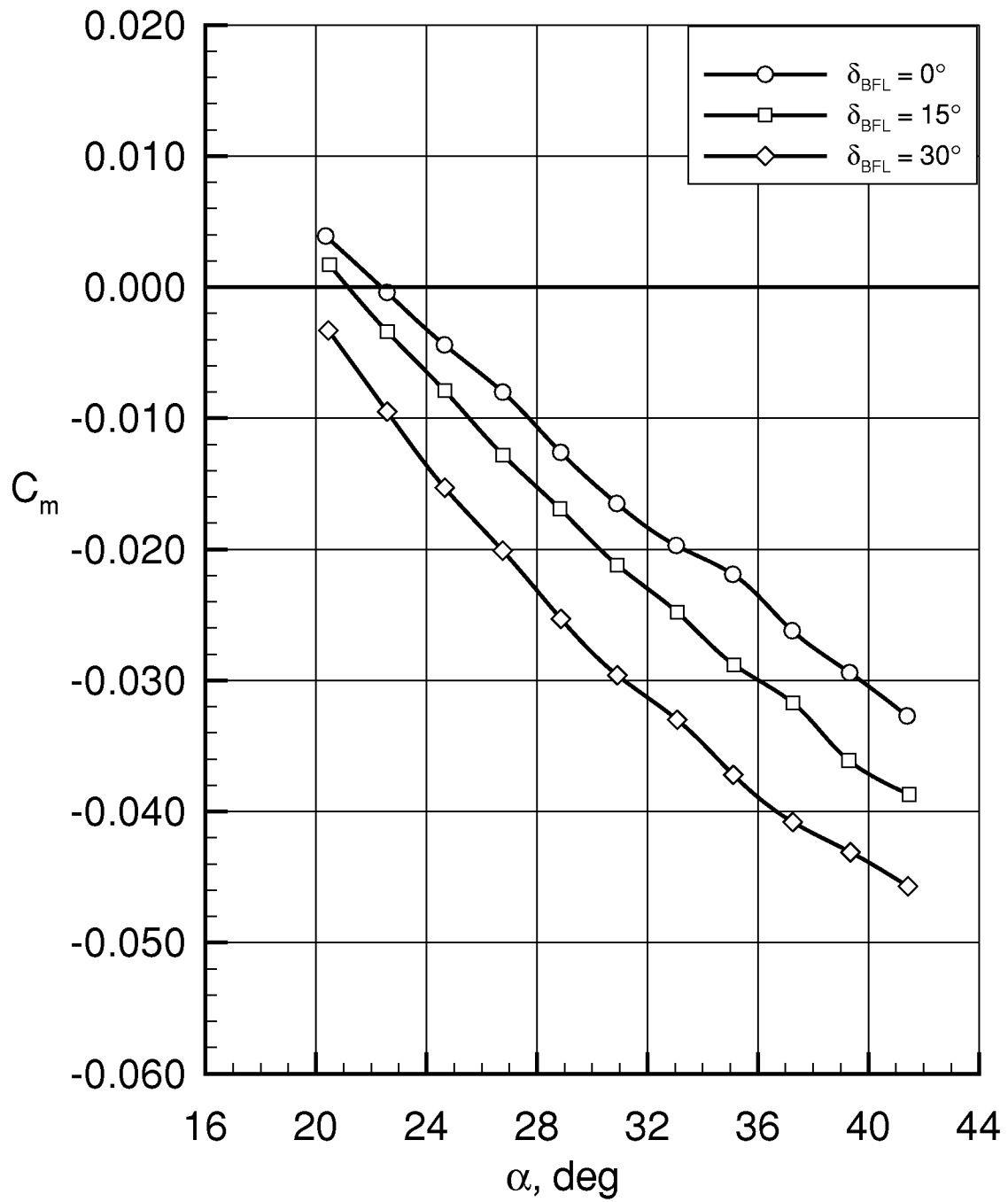
(d) C_m versus angle of attack.

Figure 10.- Concluded.
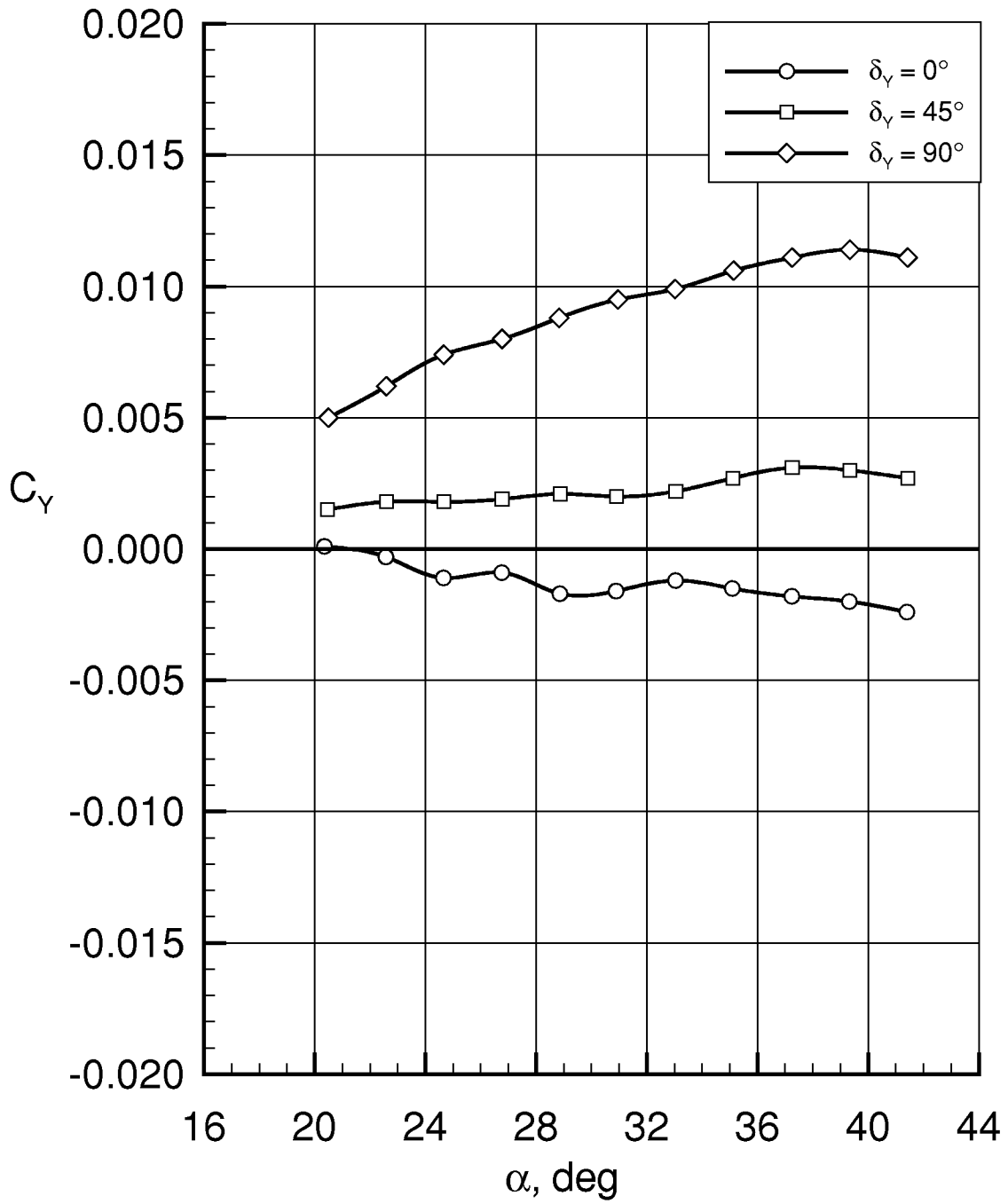
(a) C_Y versus angle of attack.

Figure 11.- Effect of yaw controller deflection on the lateral and longitudinal characteristics of the model.

(b) C_n versus angle of attack.

Figure 11.- Continued.

(c) C_l versus angle of attack.

Figure 11.- Continued.
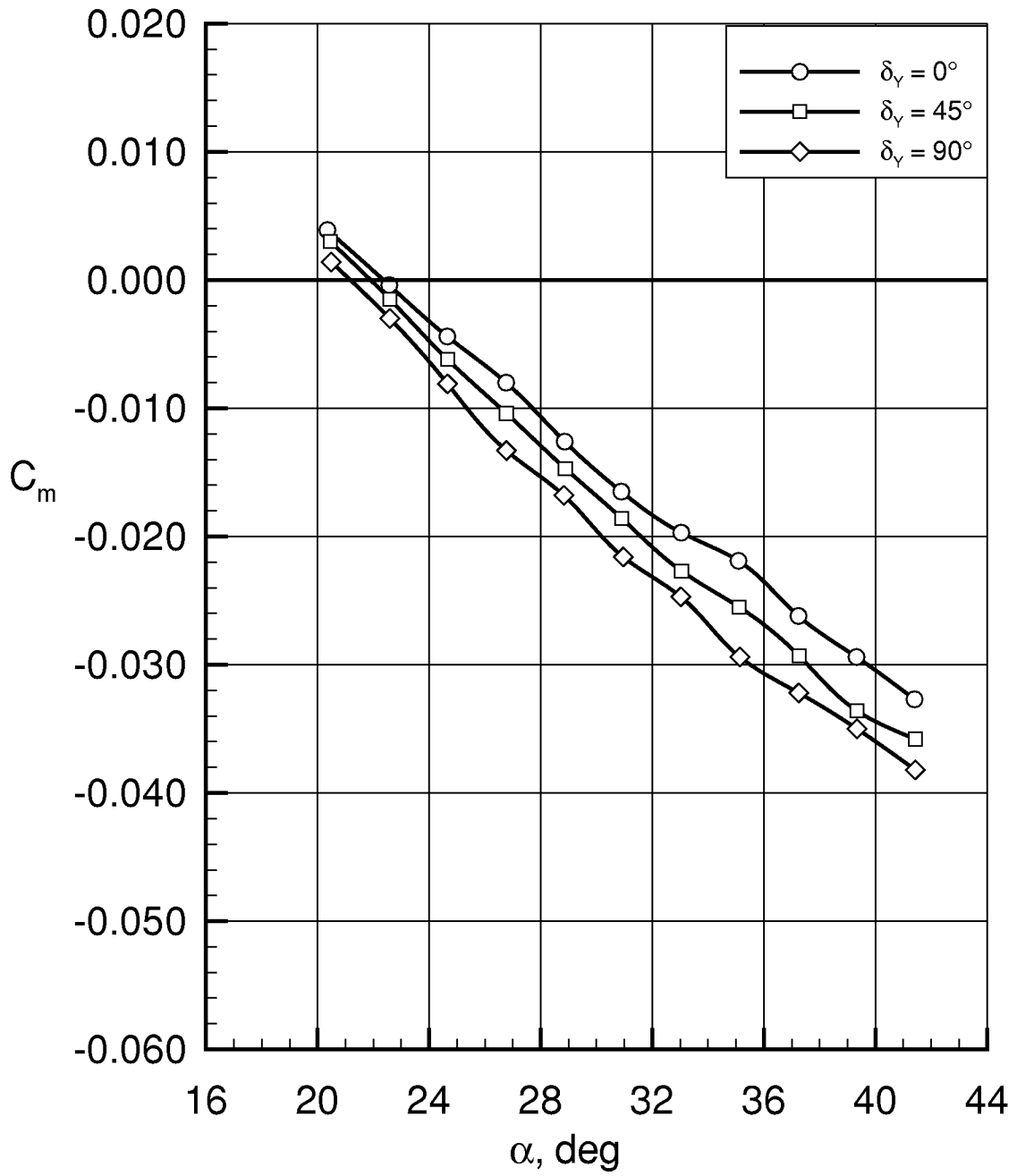
(d) C_m versus angle of attack.

Figure 11.- Concluded.
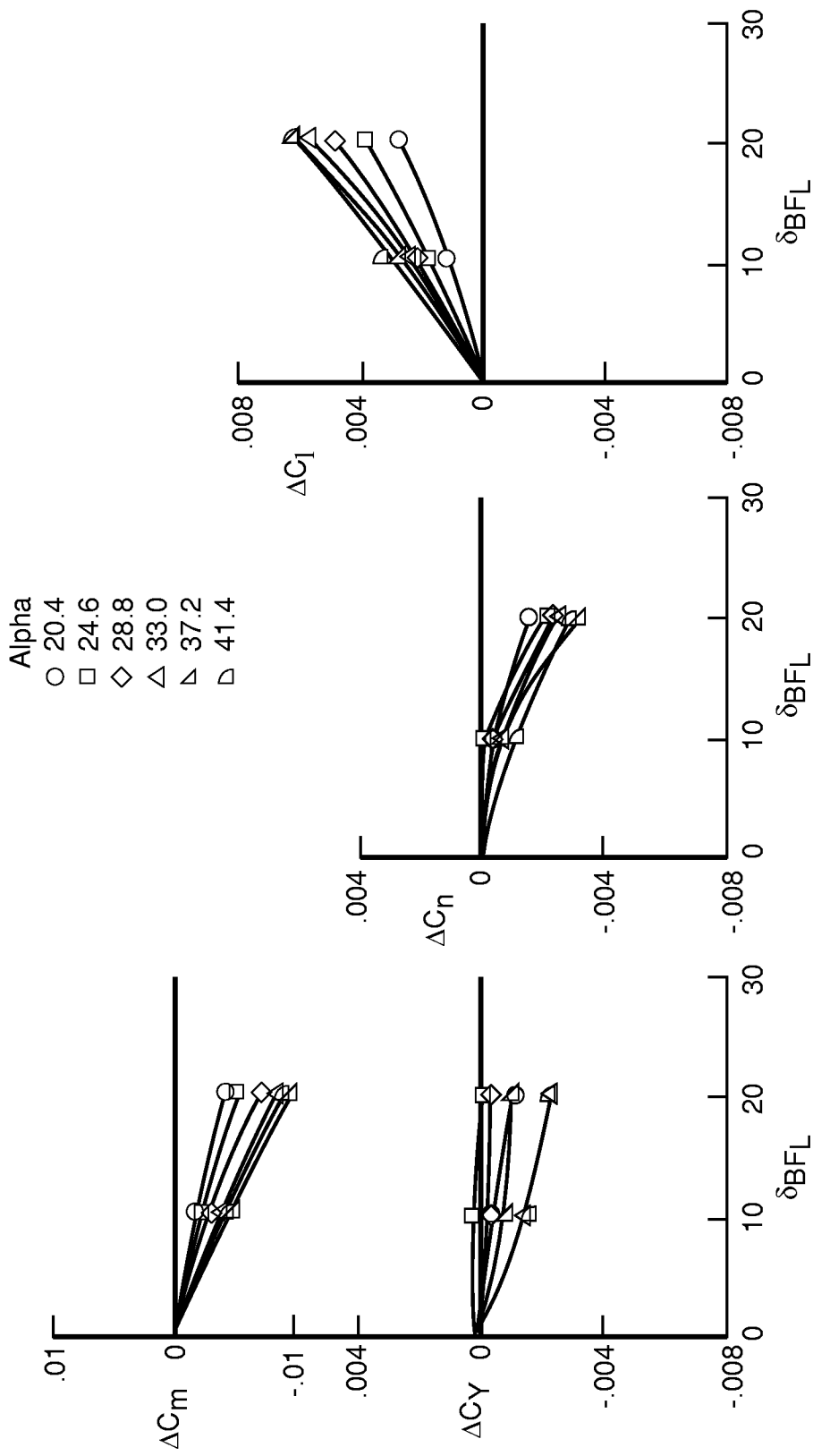
Figure 12. Roll control effectiveness of the left-hand body flap at several angles of attack. $\beta = 0°$.
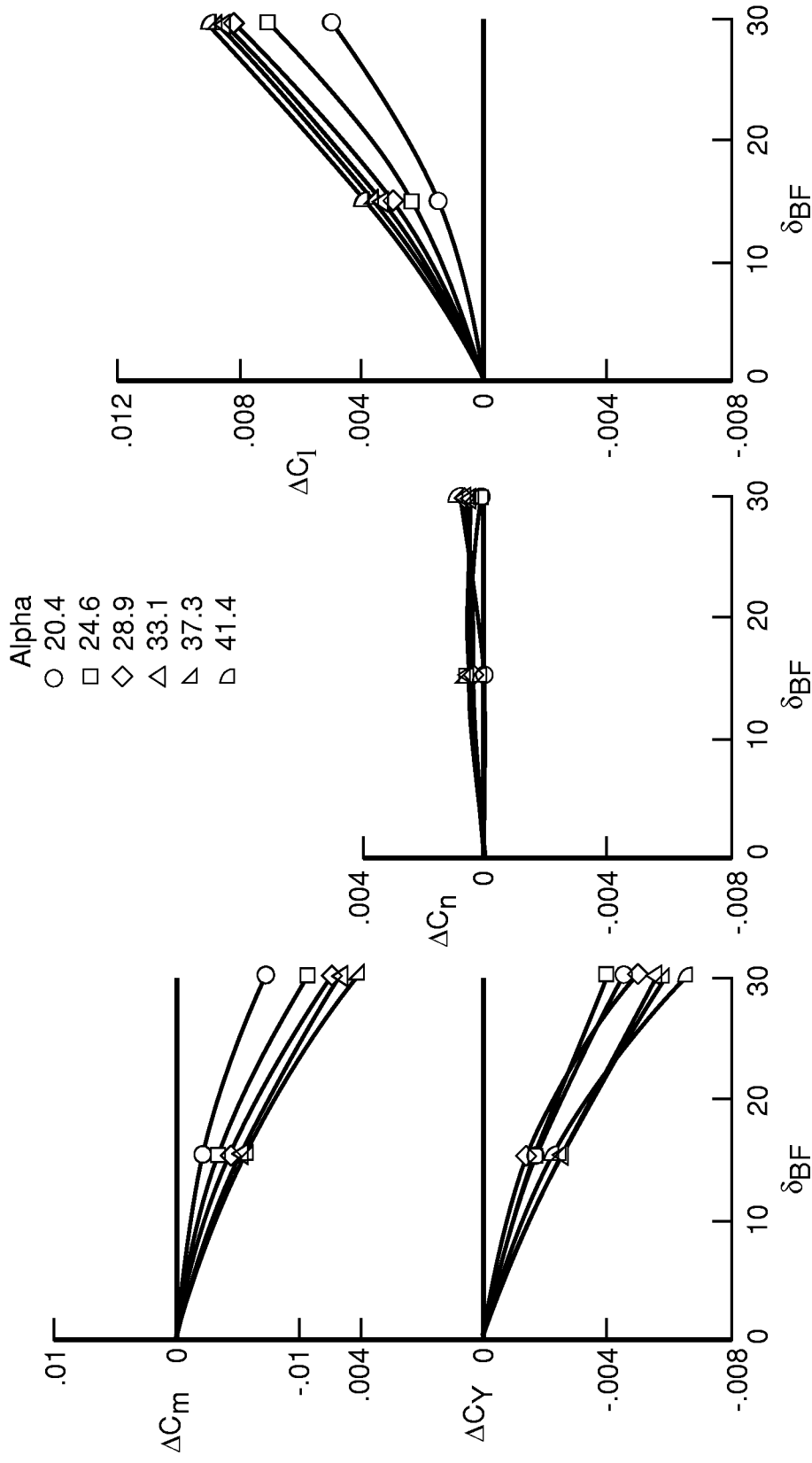
Figure 13. Roll control effectiveness of the left-hand body flap with the hinge line skewed 25° at several angles of attack. β = 0°.
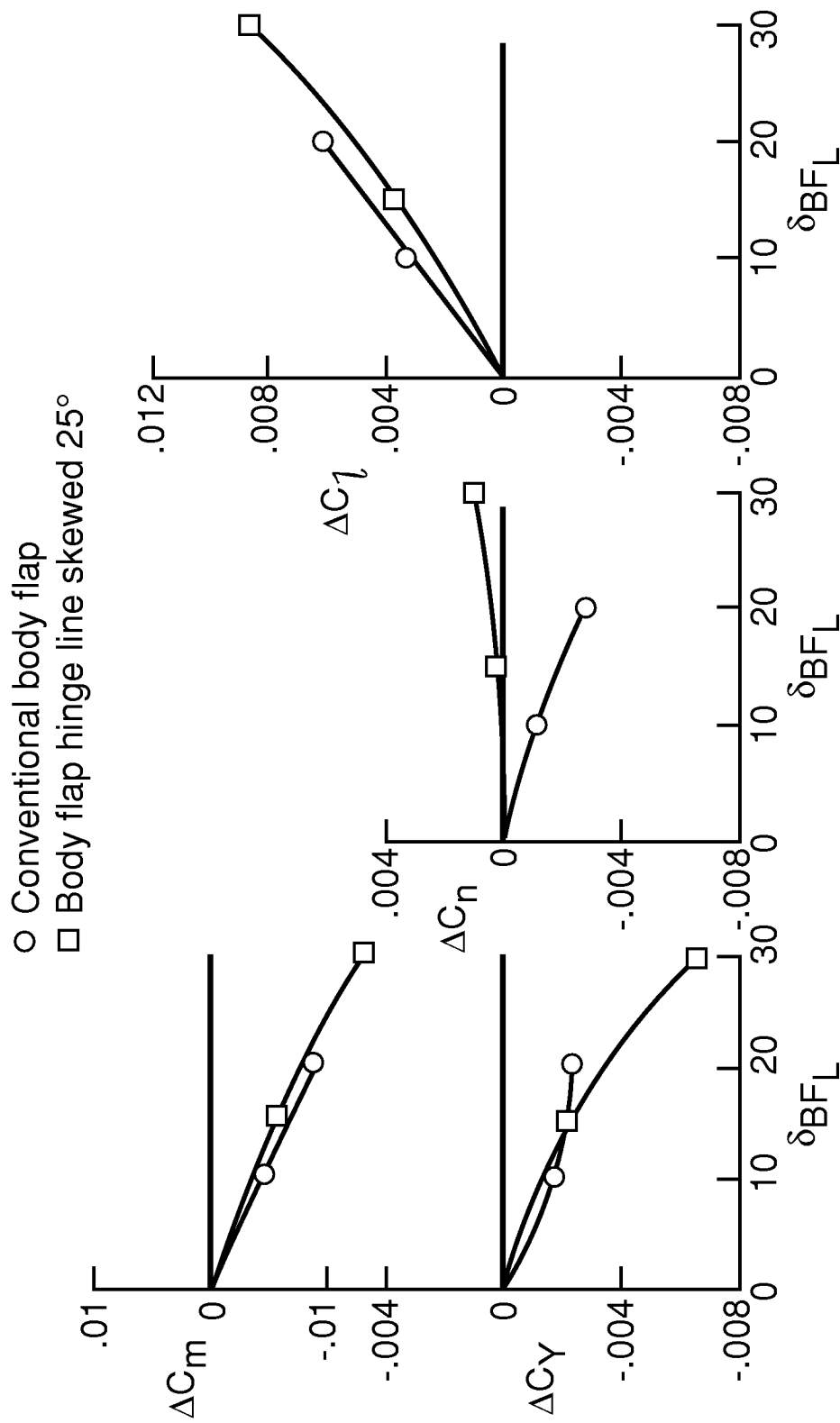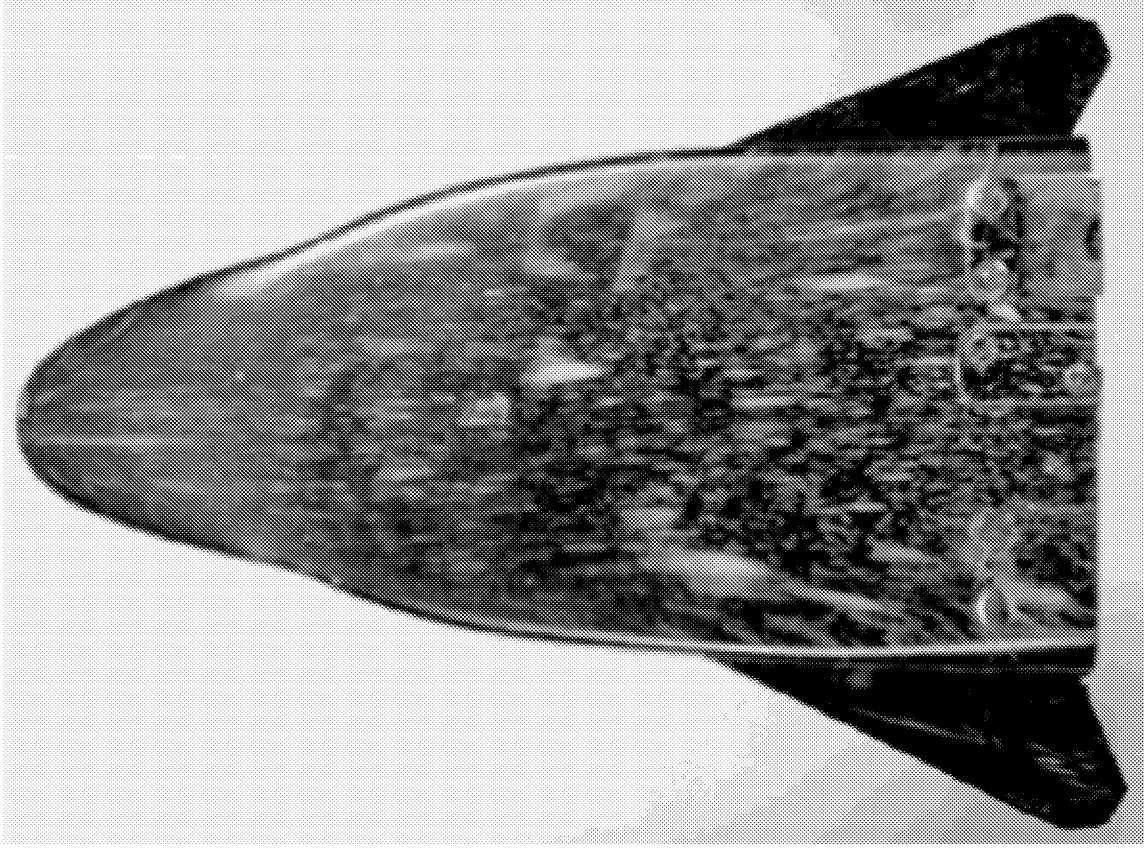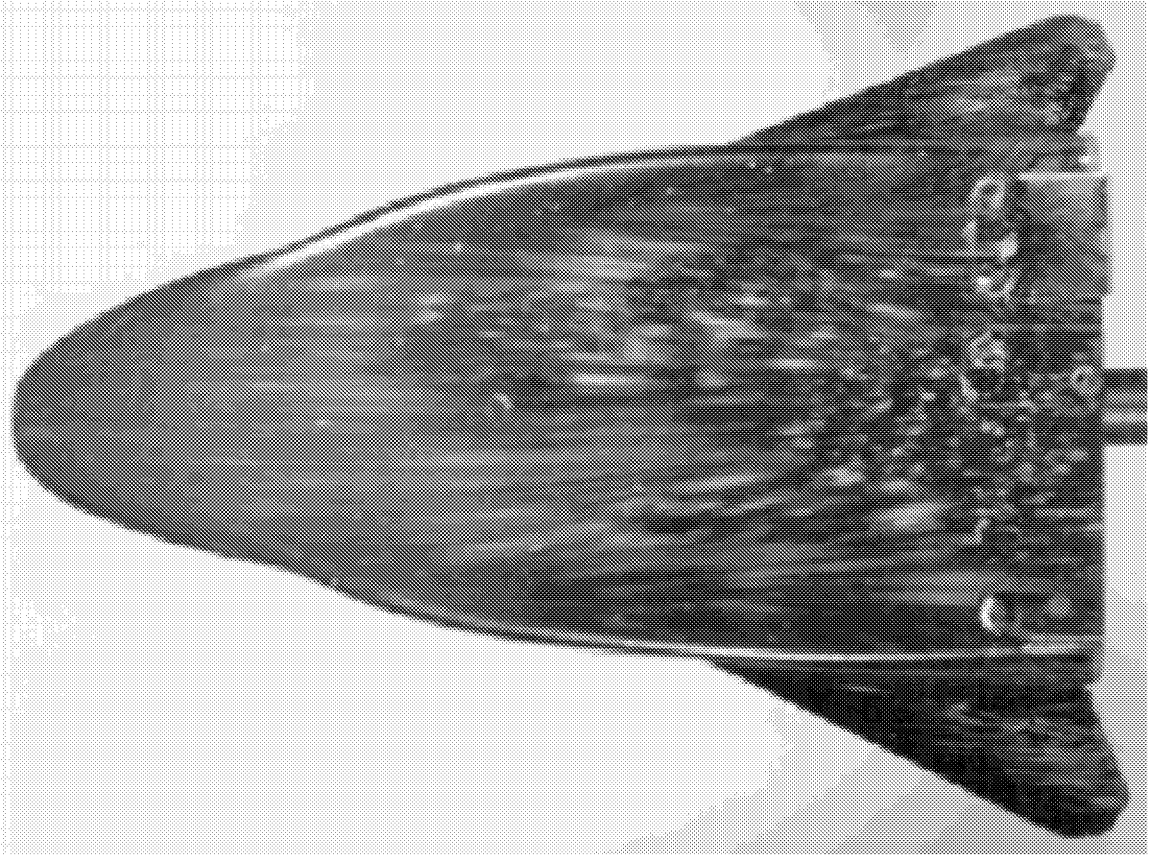
Figure 14. Comparison of the roll effectiveness of the conventional left-band body flap with that of the body flap with the hinge line skewed 25°. $\alpha = 41.4°$, $\beta = 0°$
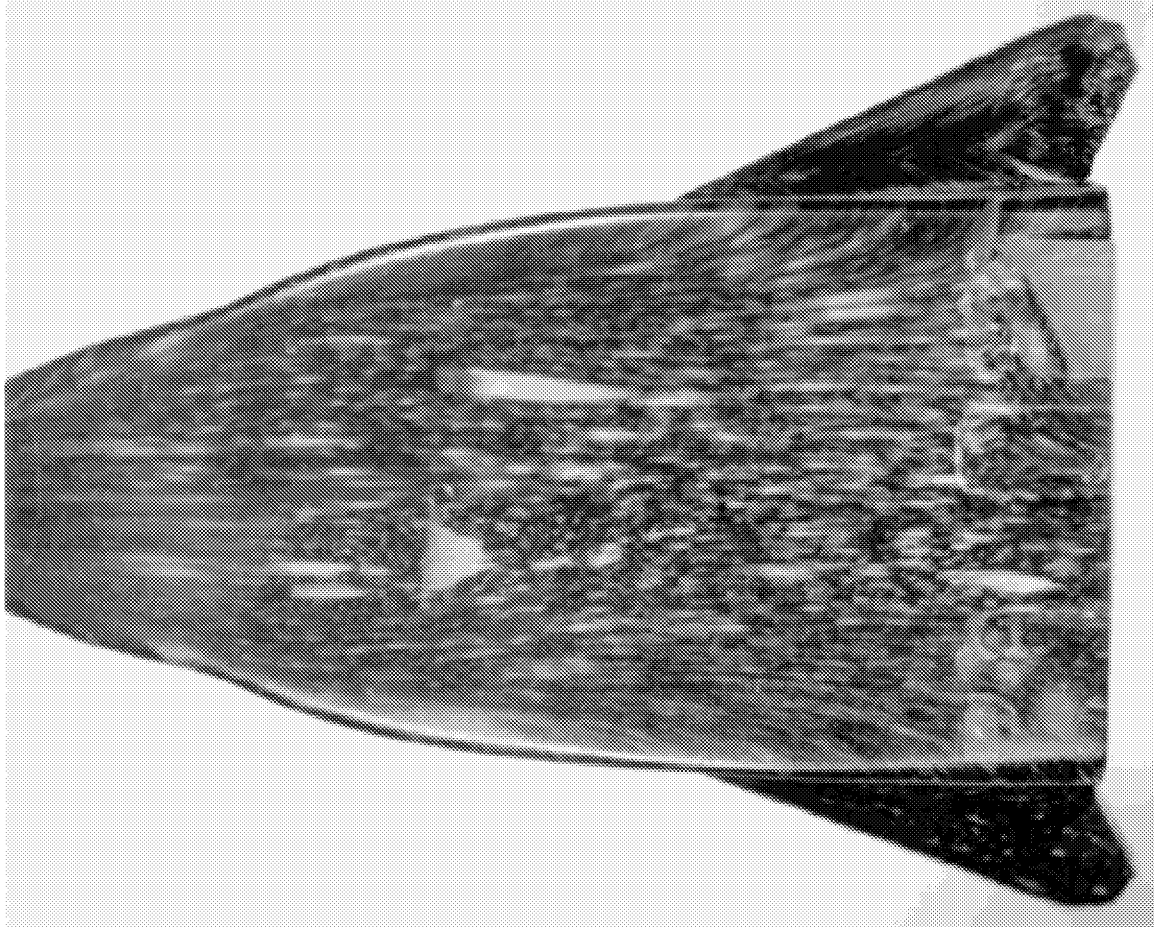
(a) Conventional hinge line, $\delta BF = 10°$, $\alpha = 30°$.

Figure 15. Surface oil-flow patterns on the bottom of the model with the right-hand body flap deflected. $R = 2.2 \times 10$ per ft.

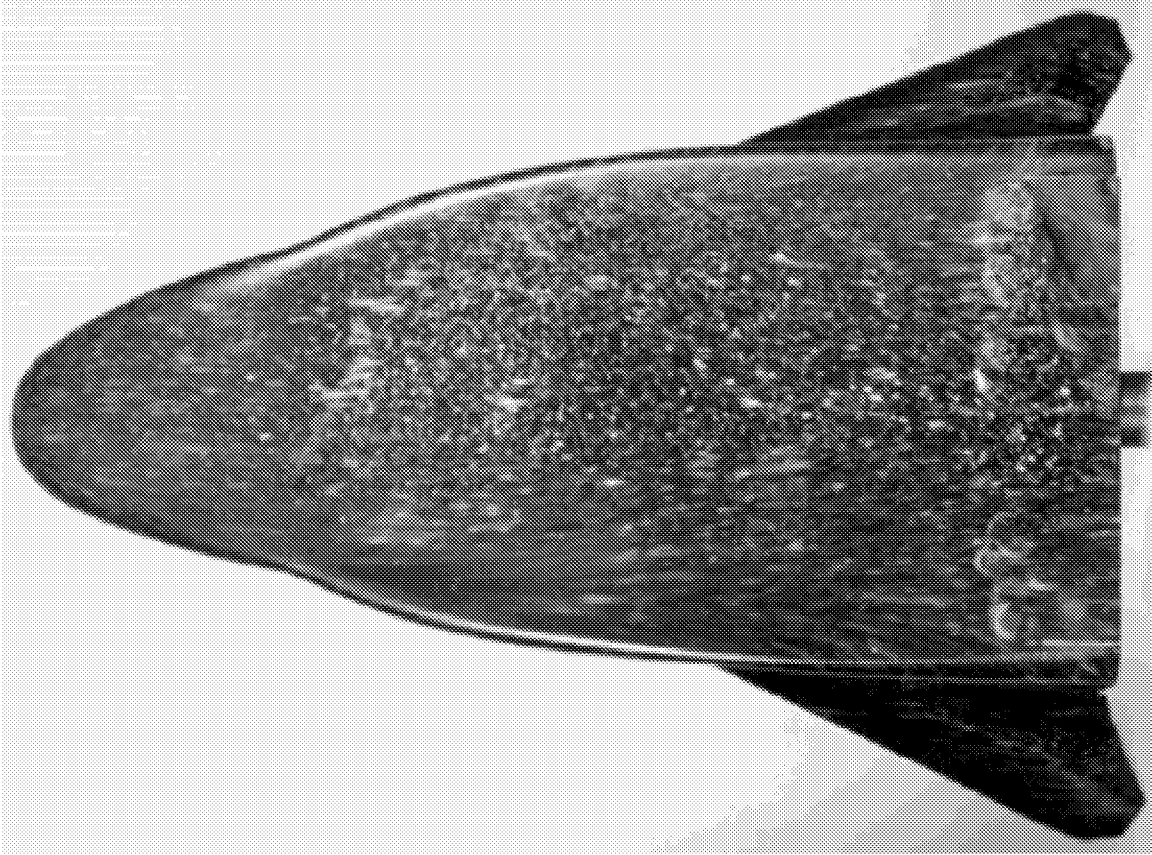(b) Conventional hinge line, $\delta BF = 10°$, $\alpha = 20°$.

Figure 15. Continued.

(c) Skewed hinge line, $\delta BF = 15°$, $\alpha = 30°$.

Figure 15. Continued.

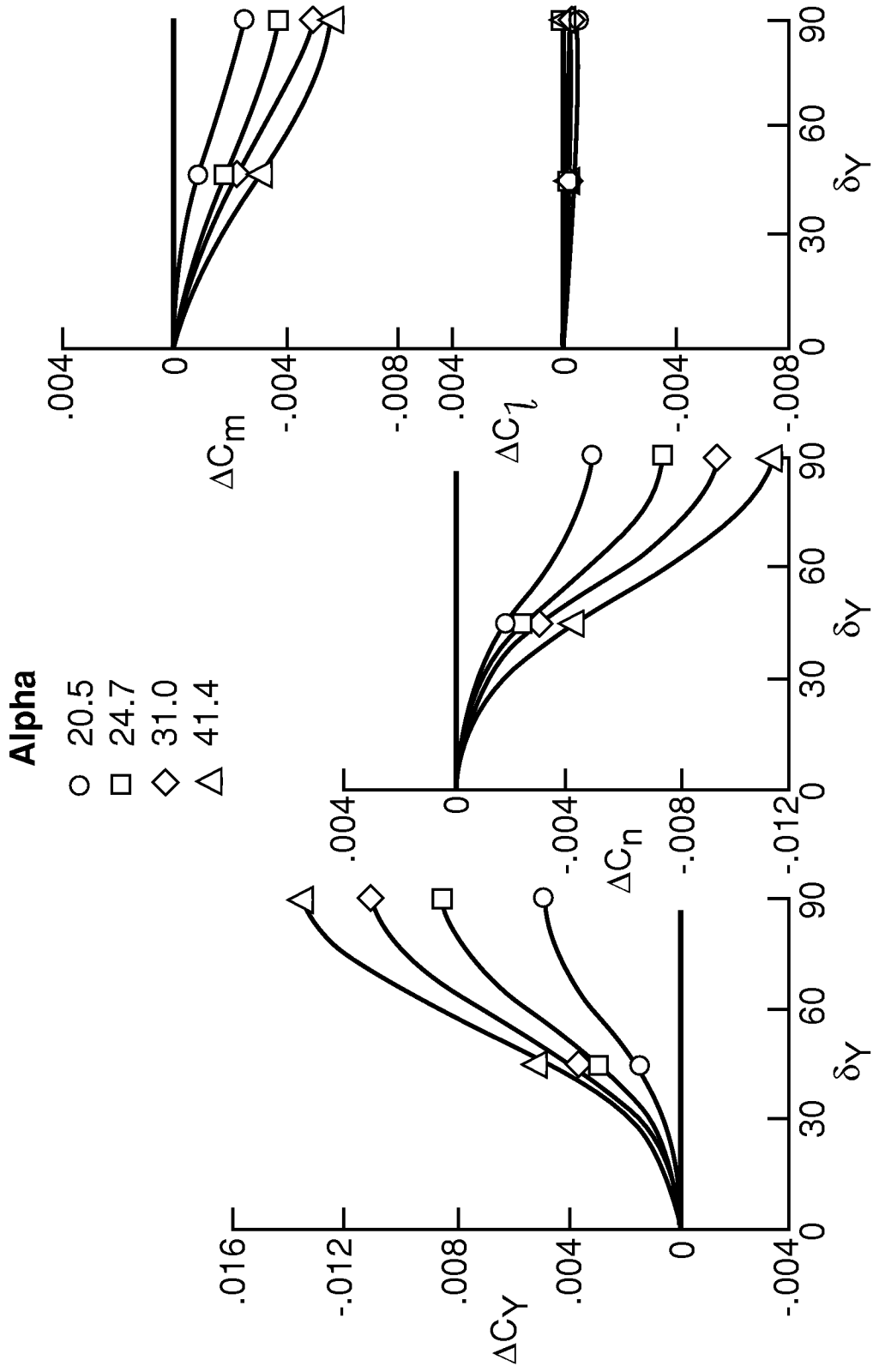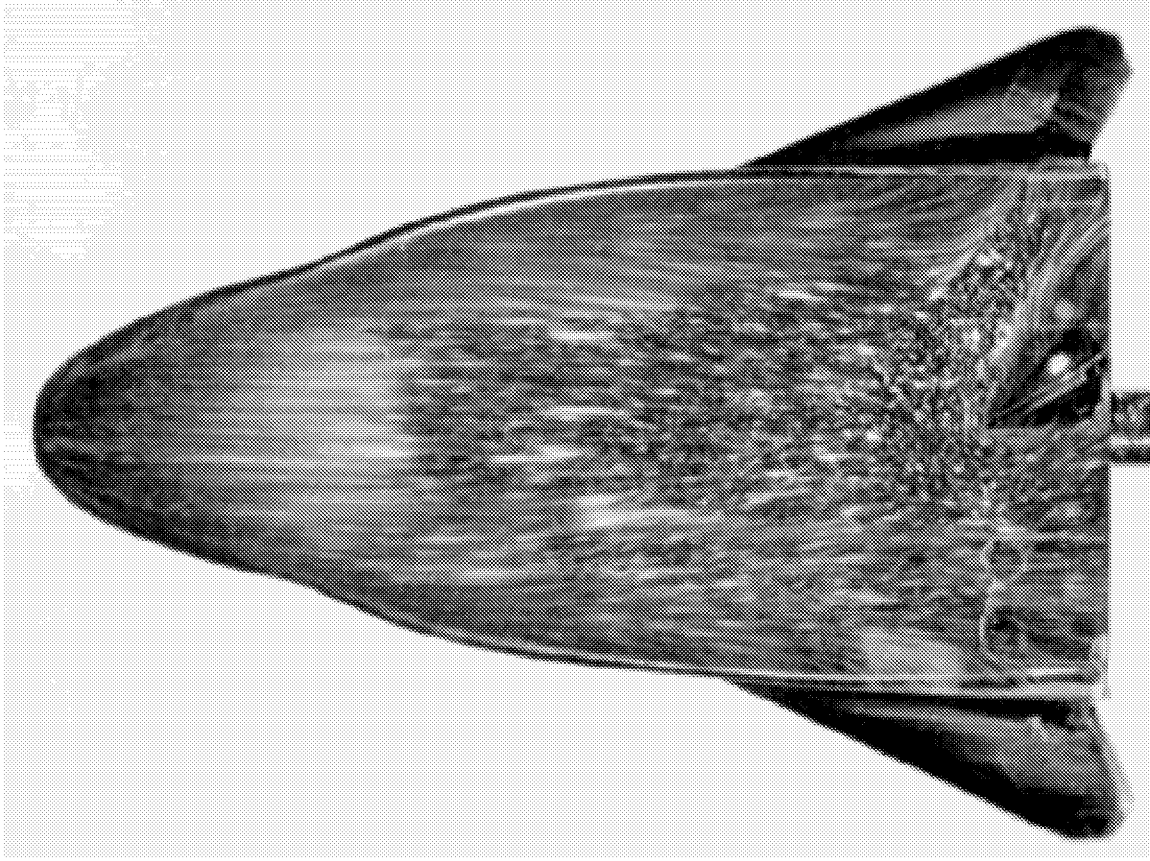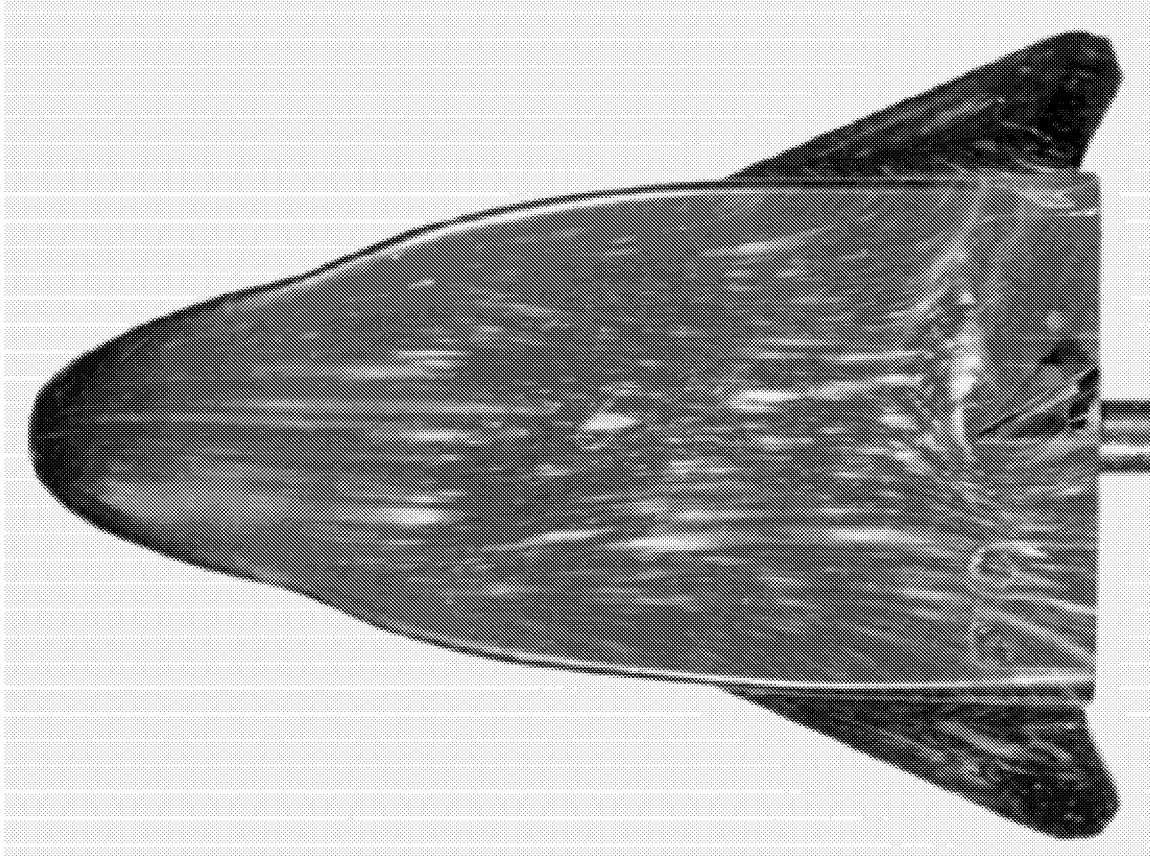(d) Skewed hinge line, δBF = 15°, α = 20°.

Figure 15. Concluded.

Figure 16. Control effectiveness of the body-mounted yaw controller at several angles of attack. β = 0°.

51
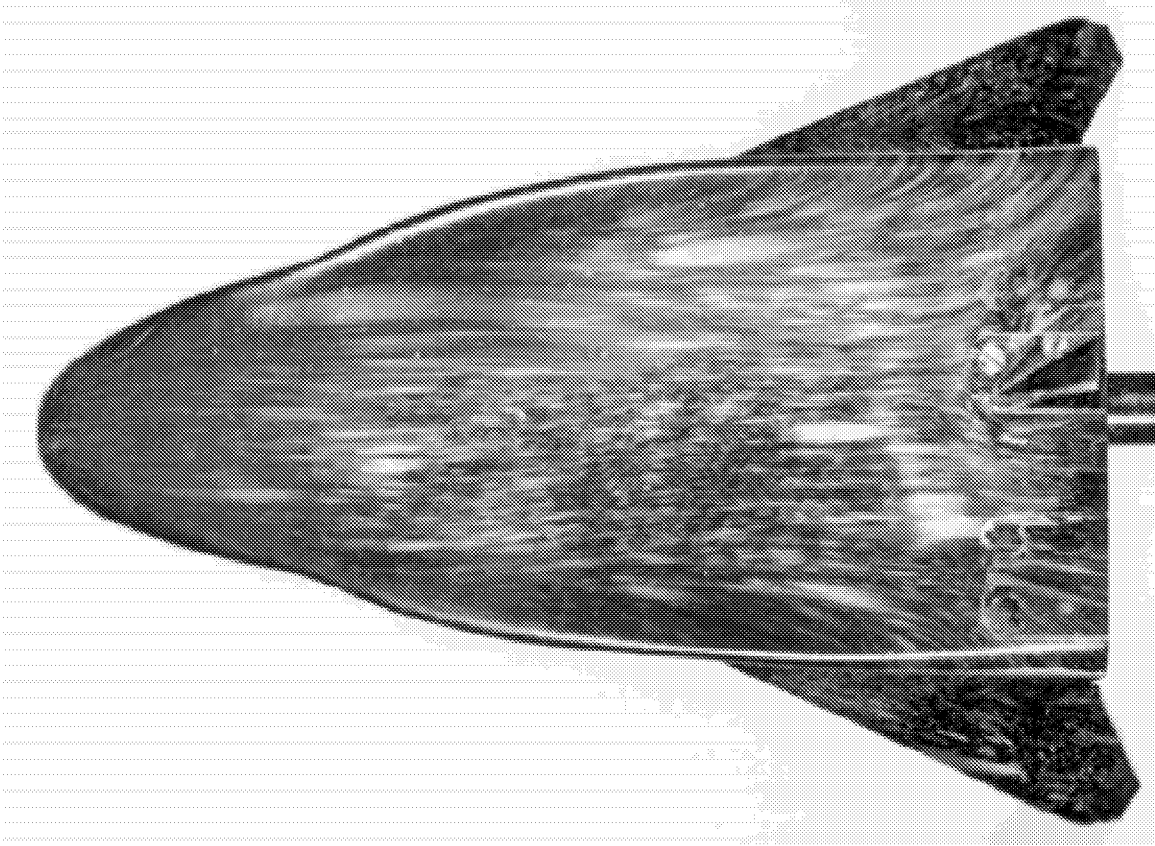
(a) $\delta Y = 90°$, $\alpha = 20°$.

Figure 17. Surface oil-flow patterns on the bottom of the model with the left-hand yaw controller deflected. Photograph in the 31 Inch Mach 10 tunnel. $R = 2.2 \times 10^6$.

(b) $\delta Y = 90°$, $\alpha = 30°$.

Figure 17. Continued.

(c) $\delta Y = 45°$, $\alpha = 30°$.

Figure 17. Concluded.

REPORT DOCUMENTATION PAGE

Public reporting burden for this collection of information is estimated to average 1 hour per response, including the time for reviewing instructions, searching existing data sources, gathering and maintaining the data needed, and completing and reviewing the collection of information. Send comments regarding this burden estimate or any other aspect of this collection of information, including suggestions for reducing this burden, to Washington Headquarters Services, Directorate for Information Operations and Reports, 1215 Jefferson Davis Highway, Suite 1204, Arlington, VA 22202-4302, and to the Office of Management and Budget, Paperwork Reduction Project (0704-0188), Washington, DC 20503.

1. AGENCY USE ONLY (Leave blank)	2. REPORT DATE	3. REPORT TYPE AND DATES COVERED
	September 1999	Technical Memorandum

4. TITLE AND SUBTITLE
Aerodynamic Characteristics and Control Effectiveness of the HL-20 Lifting Body Configuration at Mach 10 in Air

5. FUNDING NUMBERS
WU 242-80-01-01

6. AUTHOR(S)
William I. Scallion

7. PERFORMING ORGANIZATION NAME(S) AND ADDRESS(ES)
NASA Langley Research Center
Hampton, VA 23681-2199

8. PERFORMING ORGANIZATION REPORT NUMBER
L-17867

9. SPONSORING/MONITORING AGENCY NAME(S) AND ADDRESS(ES)
National Aeronautics and Space Administration
Washington, DC 20546-0001

10. SPONSORING/MONITORING AGENCY REPORT NUMBER
NASA/TM-1999-209357

11. SUPPLEMENTARY NOTES

12a. DISTRIBUTION/AVAILABILITY STATEMENT
Unclassified-Unlimited
Subject Category 02, 08, and 15   Distribution: Standard
Availability: NASA CASI (301) 621-0390

12b. DISTRIBUTION CODE

13. ABSTRACT (Maximum 200 words)
A 0.0196-scale model of the HL-20 lifting-body, one of several configurations proposed for future crewed spacecraft, was tested in the Langley 31-Inch Mach 10 Tunnel. The purpose of the tests was to determine the effectiveness of fin-mounted elevons, a lower surface flush-mounted body flap, and a flush-mounted yaw controller at hypersonic speeds. The nominal angle-of-attack range, representative of hypersonic entry, was 2 deg to 41 deg, the sideslip angles were 0 deg, 2 deg, and -2 deg, and the test Reynolds number was 1.06×10^6 based on model reference length. The aerodynamic, longitudinal, and lateral control effectiveness along with surface oil flow visualizations are presented and discussed. The configuration was longitudinally and laterally stable at the nominal center of gravity. The primary longitudinal control, the fin-mounted elevons, could not trim the model to the desired entry angle of attack of 30 deg. The lower surface body flaps were effective for roll control and the associated adverse yawing moment was eliminated by skewing the body flap hinge lines. A yaw controller, flush-mounted on the lower surface, was also effective, and the associated small rolling moment was favorable.

14. SUBJECT TERMS
Lifting body; Aerodynamics; Stability; Control

15. NUMBER OF PAGES
59

16. PRICE CODE
A04

17. SECURITY CLASSIFICATION OF REPORT	18. SECURITY CLASSIFICATION OF THIS PAGE	19. SECURITY CLASSIFICATION OF ABSTRACT	20. LIMITATION OF ABSTRACT
Unclassified	Unclassified	Unclassified	UL